Low-temperature evolution of the Morondava rift basin shoulder in western Madagascar: An apatite fission track study

Jörg Giese,[1,2,3] Diane Seward,[4] and Guido Schreurs[1]

Received 13 April 2011; revised 7 January 2012; accepted 9 January 2012; published 23 March 2012.

[1] The evolution of the rift shoulder and the sedimentary sequence of the Morondava basin in western Madagascar was mainly influenced by a Permo-Triassic continental failed rift (Karroo rift), and the early Jurassic separation of Madagascar from Africa. Karroo deposits are restricted to a narrow corridor along the basement-basin contact and parts of this contact feature a steep escarpment. Here, apatite fission track (AFT) analysis of a series of both basement and sediment samples across the escarpment reveals the low-temperature evolution of the exhuming Precambrian basement in the rift basin shoulder and the associated thermal evolution of the sedimentary succession. Seven basement and four Karroo sediment samples yield apparent AFT ages between ~330 and ~215 Ma and ~260 and ~95 Ma, respectively. Partially annealed fission tracks and thermal modeling indicate post-depositional thermal overprinting of both basement and Karroo sediment. Rocks presently exposed in the rift shoulder indicate temperatures of >60°C associated with this reheating whereby the westernmost sample in the sedimentary plain experienced almost complete resetting of the detrital apatite grains at temperatures of about ~90–100°C. The younging of AFT ages westward indicates activity of faults, re-activating inherited Precambrian structures during Karroo sedimentation. Furthermore, our data suggest onset of final cooling/exhumation linked to (1) the end of Madagascar's drift southward relative to Africa during the Early Cretaceous, (2) activity of the Marion hot spot and associated Late Cretaceous break-up between Madagascar and India, and (3) the collision of India with Eurasia and subsequent re-organization of spreading systems in the Indian Ocean.

Citation: Giese, J., D. Seward, and G. Schreurs (2012), Low-temperature evolution of the Morondava rift basin shoulder in western Madagascar: An apatite fission track study, *Tectonics*, *31*, TC2009, doi:10.1029/2011TC002921.

1. Introduction

[2] The west coast of Madagascar features three major sedimentary basins of Phanerozoic age, the Diego-Suarez (or Ambilobe) basin in the north, the crescent shaped Mahajanga basin in the northwest and the Morondava basin in the west and southwest (Figure 1). The Morondava basin is the largest and oldest of these basins, extending into the Mozambique Channel to the west [e.g., *Coffin and Rabinowitz*, 1988, 1992] and is bound to the east by Precambrian crystalline basement [e.g., *de Wit*, 2003]. The evolution of the basin is mainly influenced by three major events: (1) a Permo-Triassic continental failed rift [e.g., *Clark*, 1998; *Geiger et al.*, 2004], also referred to as the Karroo (failed) rift [e.g., *Montenat et al.*, 1996; *Bremer*, 2005]; (2) the early [*Clark*, 1998; *Geiger et al.*, 2004] to late Middle Jurassic [*Coffin and Rabinowitz*, 1988; *Rabinowitz and Woods*, 2006] separation of Madagascar from eastern Africa [*Coffin and Rabinowitz*, 1992]; and (3) the break-up from India in the Late Cretaceous [*Plummer*, 1996; *Rabinowitz and Woods*, 2006; *Ali and Aitchison*, 2008] which was accompanied by extensive volcanism on either side of the island [*Rasamimanana et al.*, 1998; *Torsvik et al.*, 2000] and coincident with activity of the Marion hot spot [*Storey*, 1995; *Storey et al.*, 1995; *Torsvik et al.*, 1998]. Finally, in Cenozoic times extension affected the Morondava basin, where existing faults were partially reactivated and active faulting is now present [*Piqué et al.*, 1999b].

[3] Today, the basement-basin contact in the northern and central parts of the Morondava basin is marked by a striking escarpment, locally displaying more than 1000 m of altitude difference from the sedimentary plain to the basement plateau. Further southwards along strike of the contact, this difference in altitude diminishes until a smooth topographical transition from the sediments onto the basement is observed.

[4] Since its separation from eastern Africa in Jurassic times, the western margin of Madagascar has remained "relatively" stable for a long period of time, i.e., it is not considered to have been part of an active tectonic regime, but has always occupied a passive tectonic setting, although there is clearly some later Neogene tectonic activity. Apatite fission track (AFT) studies might provide us with insights on far-field events (for example related to large-scale plate

[1]Institute of Geological Sciences, University of Bern, Bern, Switzerland.
[2]Institut für Geologie und Paläontologie, Westfälische Wilhelms-Universität Münster, Münster, Germany.
[3]Now at Louis Ingenieurgeologie GmbH, Weggis, Switzerland.
[4]School of Geography, Environment and Earth Sciences, Victoria University of Wellington, Wellington, New Zealand.

0278-7407/12/2011TC002921

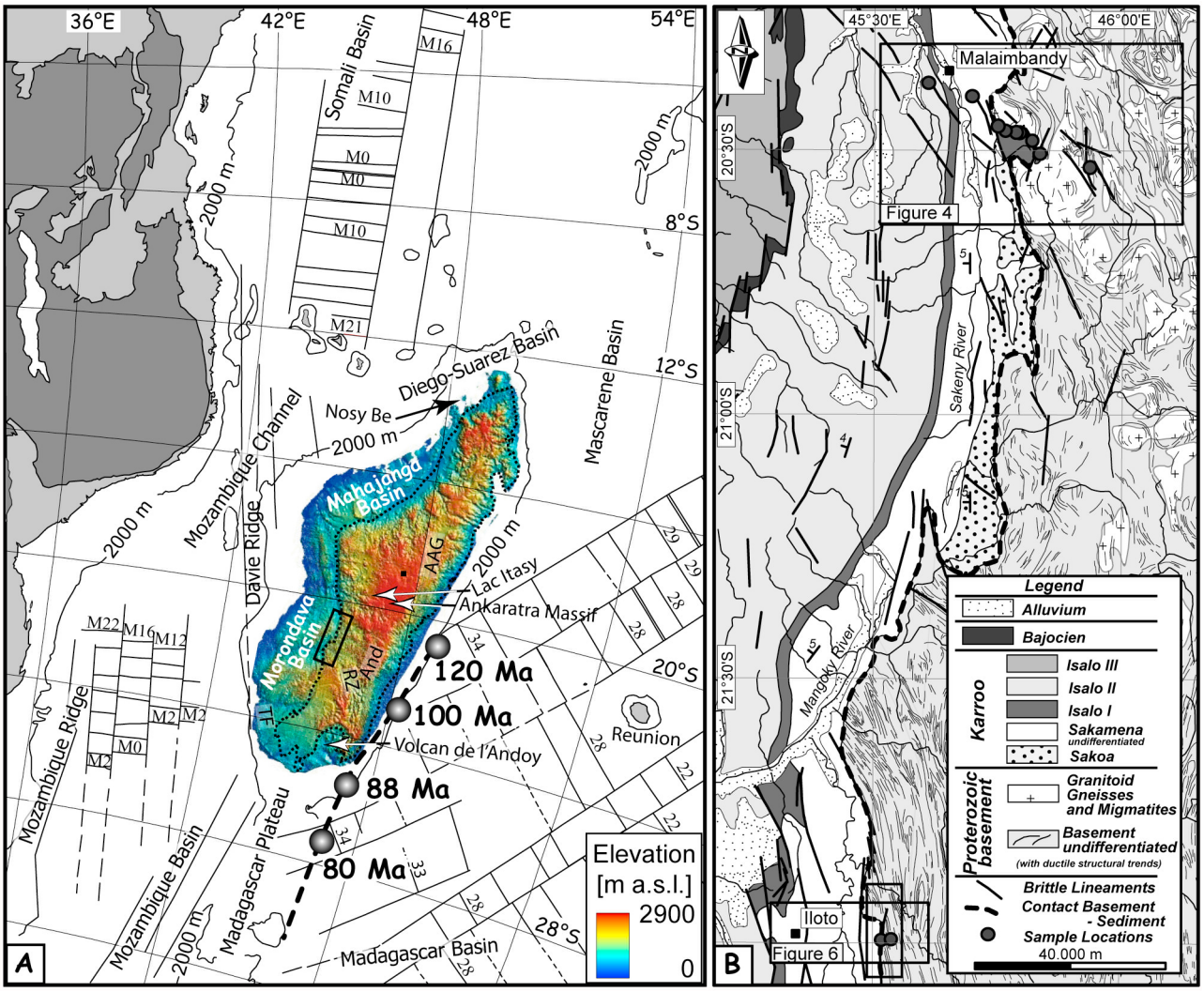

Figure 1. (a) Digital elevation model SRTM [*USGS*, 2004] showing Madagascar's current position with magnetic anomalies (modified after *UNESCO* [1990]). Shaded circles indicate the proposed positions and times of the Marion hot spot underneath Madagascar [*Storey et al.*, 1995; *Torsvik et al.* 1998]. Box indicates position of Figure 1b. AAG, Alaotra-Ankay-Graben; And, Andringitra massif; RZ, Ranotsara Zone; TF, Tulear Fault. Figure 1a is modified after *Seward et al.* [2004]. (b) Geological map of the central eastern Morondava basin (modified after *Bésairie* [1969a]).

tectonic changes) that occurred during the time that western Madagascar remained "inactive."

[5] Previous apatite fission track studies in Madagascar focused on either basement rocks [*Seward et al.*, 1998, 1999, 2000a, 2004; *Emmel et al.*, 2004, 2006a, 2008, *Jöns et al.*, 2009] or sedimentary rocks [*Emmel et al.*, 2006b]. Here we report the results of AFT analysis of both basement and sedimentary rocks sampled along the eastern margin of the central Morondava basin (Figure 1). Part of the low-temperature history of the basement rocks is constrained by the onlap of sediments of known stratigraphic age. Samples of sedimentary rocks of different stratigraphic ages and from varying altitudes partly alternating with basement rocks were collected along a transect across the basin-basement contact. Modeling of the thermal evolution is used to identify potential thermotectonic events responsible for the present structural and morphological architecture, to constrain the cooling/exhumation history of the basin shoulder and to provide clues for potential hydrocarbon formation in the sediments close to the basin-basement contact.

1.1. Geodynamic Evolution of Syn- and Post Gondwana Break-Up

1.1.1. Separation of Madagascar From Eastern Africa

[6] The development of the Phanerozoic sedimentary basins along the west coast of Madagascar is linked to its separation from Africa. Dispersal commenced with Karroo rifting in the southern part of the Morondava basin propagating northward [*Montenat et al.*, 1996; *Piqué et al.*, 1999a]. The structural style changed from the development of local pull-apart basins during deposition of the oldest sedimentary units of Late Carboniferous to Early Permian times, the

Sakoa Group, to transtensional conditions and widening of the depositional centers during sedimentation of the Sakamena Group (Late Permian to Middle Triassic) and later orthogonal extension followed by thermal subsidence during deposition of mainly siliciclastic deposits of the Isalo Group in Middle Triassic to Early Jurassic times [*Piqué et al.*, 1999a; *Schandelmeier et al.*, 2004].

[7] Subsequently, the rift locus in the Morondava basin shifted westward and after a gap in sedimentation, final separation between Madagascar and Eastern Africa occurred during the Middle to Late Jurassic [*Clark*, 1998; *Geiger et al.*, 2004; *Rabinowitz et al.*, 1983; *Coffin and Rabinowitz*, 1992; *Bouysse et al.*, 2004]. The southward drift of Madagascar along the Davie Ridge in the Mozambique Channel [*Coffin and Rabinowitz*, 1988; *Malod et al.*, 1991] resulted in the formation of a true passive margin in the northern Mahajanga basin and the development of a transform margin in the Morondava basin [*Montenat et al.*, 1996; *Piqué*, 1999]. The present-day position of Madagascar relative to Africa was achieved when seafloor spreading ceased in the Somali basin and occurred either at ∼118 Ma [*Ségoufin and Patriat*, 1980; *Cochran*, 1988; *Bouysse et al.*, 2004] or at ∼133 Ma [*Rabinowitz et al.*, 1983; *Eagles and König*, 2008].

1.1.2. Break-Up Between Madagascar and India-Seychelles

[8] The break-up between Madagascar and India-Seychelles in Late Cretaceous times (88 Ma [*Storey*, 1995; *Storey et al.*, 1995], 85 Ma [*Chand and Subrahmanyam*, 2003], ∼84 Ma [*Rabinowitz and Woods*, 2006], 85–90 Ma [*Ali and Aitchison*, 2008]) coincides with the extrusion of large amounts of predominantly mafic volcanics [e.g., *Storey et al.*, 1995, 1997; *Rasamimanana et al.*, 1998; *Torsvik et al.*, 1998; *Meert and Tamrat*, 2006; *Bardintzeff et al.*, 2010]. It has been suggested that the whole island of Madagascar was covered during the (Late?) Cretaceous by tholeiitic flood-basalts and rhyolites [*Bésairie*, 1972b; *de Wit*, 2003]. This volcanism has been linked to the Marion hot spot, whose focal point at ∼90 Ma is suggested to be the Volcan de l'Androy in SE Madagascar [*Storey et al.*, 1995]. Late Cretaceous dike swarms penetrate both the basement and sediments in the Morondava basin [*de Wit*, 2003, and reference therein].

1.1.3. Post Break-Up Evolution of Madagascar

[9] After a period of relative tectonic quiescence [*Emmel et al.*, 2006b, and references therein], Neogene to present rifting commenced [e.g., *Rasamimanana et al.*, 1998; *Piqué*, 1999; *Piqué et al.*, 1999b] leading to regional NW-SE extension of the Davie Ridge [*Mougenot et al.*, 1986; *Malod et al.*, 1991] and overall E-W extension in Madagascar [*Rakotondraompiana et al.*, 1999]. N-S striking pre-existing structures in the basement were reactivated [*Piqué et al.*, 1999b] and N-S trending basins were generated, the most prominent being the Alaotra-Ankay graben system [*Laville et al.*, 1998].

[10] Lithospheric thinning affects the whole of Madagascar and is associated with Neogene [e.g., *Rasamimanana et al.*, 1998] and Quaternary to recent volcanism [e.g., *Bésairie*, 1973; *Hottin*, 1976; *Kusky et al.*, 2007] mainly in central (Ankaratra and Itasy) and northern Madagascar. Minor occurrences of Miocene volcanics occur in the western Morondava basin [*Rasamimanana et al.*, 1998; *Bardintzeff et al.*, 2001, 2010] and are associated with the active Tulear fault [*Piqué et al.*, 1999b].

2. Geological Setting

2.1. Geology of the Morondava Rift Basin Shoulder

[11] Five major lithotectonic domains of Precambrian age—from north to south the Antananarivo-, Itremo-Ikalamavony-, Anosyen-, Androyen- and Vohibory domain—flank the eastern margin of the Morondava basin (Figure 2a). These domains, separated by tectonic contacts, are characterized by unique lithological assemblages and different Neoproterozoic histories of sedimentation, metamorphism, magmatism and deformation [e.g., *Martelat et al.*, 2000; *Boger et al.*, 2009a, 2009b, 2009c] and form part of the crystalline basement that underlies the eastern two-thirds of the island of Madagascar. Except for the Vohibory domain, all other domains were intruded by granitoids between ∼580 and 530 Ma during the final stages of Gondwana amalgamation [e.g., *Tucker et al.*, 2007; *Boger et al.*, 2009a, 2009b, 2009c; *Giese et al.*, 2011]. Late Neoproterozoic to Cambrian amphibolite to granulite facies metamorphism affected most of the Malagasy basement and lasted until ∼500 Ma [e.g., *Boger et al.*, 2009a, 2009b, 2009c; *Giese et al.*, 2011].

2.2. Geology of the Morondava Basin

[12] The present thickness of the sediments in the Morondava basin is generally at a maximum in the south, thinning toward the north [*Razafimbelo*, 1987; *Coffin and Rabinowitz*, 1988]. The entire sedimentary sequence dips gently toward the west such that the oldest deposits are exposed in the SE of the Morondava basin and the sedimentary units become progressively younger westward [e.g., *Bésairie*, 1972b]. The sedimentary succession associated with the Permo-Triassic rift is commonly referred to as the Karroo sequence [*Bésairie*, 1972b; *Razafimbelo*, 1987; *Piqué*, 1999], and includes the deposits of the Sakoa, the Sakamena and the Isalo Groups. After a hiatus in sedimentation, deposition recommenced in late Liassic times and continued until today (Figure 2b).

2.2.1. Sakoa Group: Late Carboniferous to Early Permian

[13] The Sakoa Group lies discordantly on basement and is restricted to local, structurally confined basins [*Coffin and Rabinowitz*, 1988; *Schandelmeier et al.*, 2004]. Total thickness varies dramatically from sub-basin to sub-basin, reaching up to 2000 m in the south thinning gradually until in the northern Morondava basin none is preserved [*Coffin and Rabinowitz*, 1988]. The sequence is subdivided into four units [*Bésairie*, 1972b], featuring glacial and fluvial deposits [*Hirtz*, 1950; *Bésairie*, 1972b; *Razafimbelo*, 1987; *Coffin and Rabinowitz*, 1988; *Wescott and Diggens*, 1997; *Piqué et al.*, 1999a] topped by a 20 to 30 m thick Vohitolia limestone representing the first marine transgression into the Morondava basin in Madagascar [*Wescott and Diggens*, 1997].

2.2.2. Sakamena Group: Late Permian to Middle Triassic

[14] The deposits of the Sakamena Group rest with an angular unconformity of ∼12° on either Sakoa or basement rocks [*Razafimbelo*, 1987; *Coffin and Rabinowitz*, 1988;

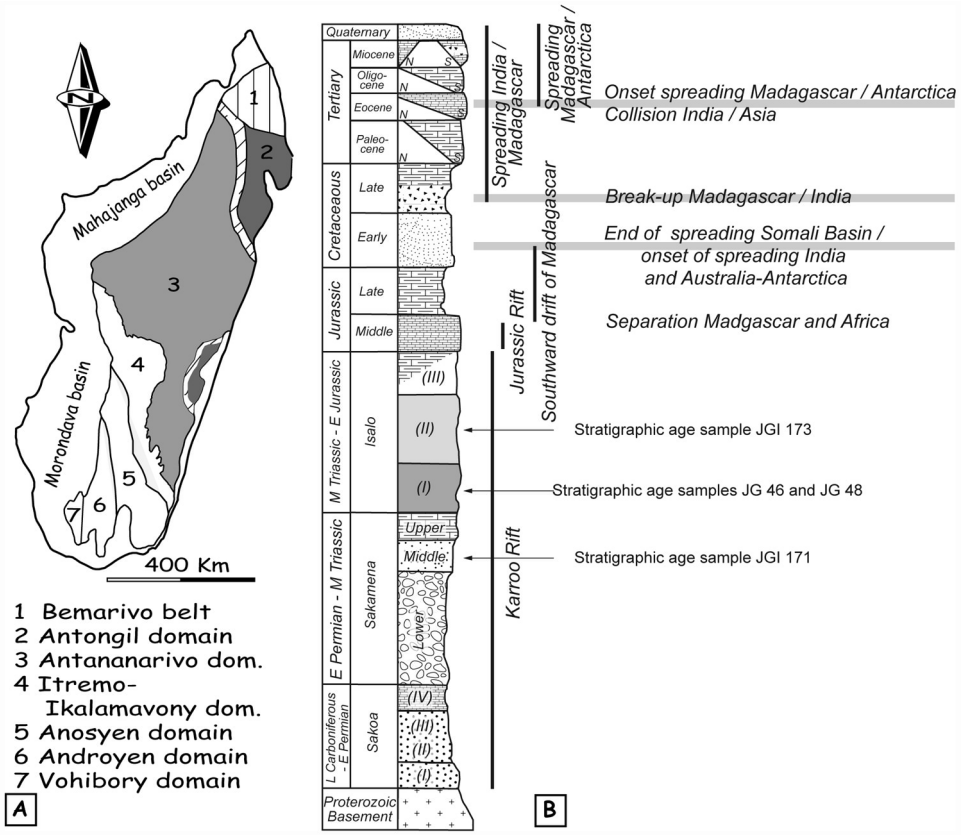

Figure 2. (a) Overview map of major lithotectonic basement domains of Madagascar [after *Bésairie*, 1969a, 1969b, 1972a; *Collins and Windley*, 2002; *Boger et al.*, 2009a, 2009b, 2009c]. (b) Schematic stratigraphic column of the Morondava basin (modified after *Piqué et al.* [1999a]). Stratigraphic ages after *Wescott and Diggens* [1997, 1998], *Piqué et al.* [1999a], and *Coffin and Rabinowitz* [1988]. Relative stratigraphic position of sedimentary AFT samples JG 46, JG 48, JGI 171, and JGI 173 indicated by arrows. Tertiary subdivisions indicate schematically varying thicknesses of the sedimentary successions between northern and southern Morondava basin. Geodynamic events after *Janssen et al.* [1995] and *Reeves and de Wit* [2000]. Light gray boxes indicate periods of onset of exhumation as indicated by the present data set (see sections 4.3 and 5.2).

Wescott and Diggens, 1998]. The maximum thickness reaches over 4000 m in the south decreasing to less than 20 m in the north [*Coffin and Rabinowitz*, 1988]. The continental deposits, as indicated by the palaeocurrent direction, were sourced from the basement to the east [*Piqué et al.*, 1999a, and references therein]. The Sakamena succession is subdivided into three units.

[15] (1) The Lower Sakamena has a coarse basal conglomerate with components of crystalline basement and Vohitolia limestone [*Coffin and Rabinowitz*, 1988]. It continues upwards as a succession of shales, sandstones and minor conglomerates of fluvial origin with minor marine limestone [*Wescott and Diggens*, 1998; *Coffin and Rabinowitz*, 1988].

[16] (2) The Middle Sakamena is a sequence of shales and minor sandstones deposited in a lagoonal or shallow lacustrine and braided river environment [*Wescott and Diggens*, 1998; *Piqué et al.*, 1999a].

[17] (3) The Upper Sakamena is an alternation of white cross-bedded sandstones with red shales [*Coffin and Rabinowitz*, 1988] deposited in similar environments to the Middle Sakamena but with overall coarsening upwards [*Wescott and Diggens*, 1998].

2.2.3. Isalo Group: Middle Triassic to Early Jurassic

[18] The Isalo Group ranges in thickness from 5000 to 6000 m in the south to 1700 m in the north [*Coffin and Rabinowitz*, 1988]. Classically, it is divided into three groups [*Bésairie*, 1972b]. The contact between the Isalo I formation and the Upper Sakamena varies locally from transitional and conformable to unconformable [*Bésairie*, 1972b; *Wescott and Diggens*, 1998]. Therefore, *Razafimbelo* [1987] argues for the continuity of sedimentation between the two and assigns the Isalo I to the uppermost Sakamena. Further, he regards the discontinuity between Isalo I and Isalo II as the major break, and the beginning of a new sedimentary cycle. The type locality, however, is the Isalo massif in the SE Morondava basin, comprising the deposits of the Isalo I. Accordingly, *Razafimbelo* [1987] locates the major occurrences of Isalo II further NW in the Makay massif and suggests renaming the deposits of the Isalo II as the Makay Group [for further discussion refer to *Razafimbelo*, 1987].

[19] For coherence, we retain the traditional tripartite division, established by *Bésairie* [1972b].

[20] (1) The Isalo I is composed of coarse grained, poorly sorted, white and gray arkosic sandstones and abundant conglomerates [*Wescott and Diggens*, 1998; *Piqué et al.*, 1999a] deposited in fluvial channels on a vast braided alluvial plain [*Wescott and Diggens*, 1998].

[21] (2) The Isalo II resting unconformably on Isalo I, and in some places directly on basement, is made up of conglomerates and fluvial sandstones [*Piqué et al.*, 1999a].

[22] (3) The Isalo III is composed of limestone, sandstones and shales and was deposited in a deltaic environment with occasional marine incursions [*Piqué et al.*, 1999a].

2.2.4. Middle Jurassic

[23] Aalenian sandstones are of continental facies and are hardly distinguishable from the older Isalo Group [*Coffin and Rabinowitz*, 1988; *Geiger et al.*, 2004]. Whether or not the deposits are related to the end of the depositional cycle of the Karroo rift and the initialization of the juvenile Jurassic rift, remains a matter of discussion (refer to discussion by *Geiger et al.* [2004]).

[24] During the Bajocian and Bathonian, marine conditions dominated in the northern part of the basin, building a 250–300 m thick carbonate platform [*Montenat et al.*, 1996] deposited in a shallow marine to tidal environment [*Montenat et al.*, 1996]. Further south a gradual transition from marine to a mixed marine-continental facies is observed [*Montenat et al.*, 1996]. Various periods of non-deposition are recognized [*Coffin and Rabinowitz*, 1988]. *Geiger et al.* [2004] interpret the early Bajocian unconformity as the Gondwana break-up unconformity and hence, regard the Bajocian and Bathonian as post-break-up strata.

2.2.5. Late Jurassic

[25] In the Late Jurassic the northern Morondava basin was governed by marine deposition. Limestones up to ~200 m gradually pass into mixed marine-continental facies in the central (up to ~500 m) and southern (up to ~900 m) Morondava basin [*Coffin and Rabinowitz*, 1988]. Major periods of non-deposition are recognized for example in the extreme south [*Coffin and Rabinowitz*, 1988]. Offshore, rhyolites, interbedded with marine deposits, were recovered from boreholes [*Coffin and Rabinowitz*, 1988].

2.2.6. Cretaceous

[26] In most parts of the Morondava basin, Early Cretaceous sediments through to the Albian are generally absent except for sporadically occurring glauconitic marls of Valanginian age [*Montenat et al.*, 1996].

[27] A thick clastic succession of predominantly continental Albo-Cenomanian deposits rests unconformably on an eroded surface [*Montenat et al.*, 1996], grading rapidly offshore into shales [*Coffin and Rabinowitz*, 1988]. Basaltic dikes, gabbroic intrusions and basaltic lava flows - dated at ~90 Ma [*Storey et al.*, 1995; *Rasamimanana et al.*, 1998; *Bardintzeff et al.*, 2001, 2010] are intercalated with the sediments [*Coffin and Rabinowitz*, 1988]. The Coniacian to Maastrichtian strata are dominantly of marine facies reaching a total of 150–200 m in thickness [*Coffin and Rabinowitz*, 1988].

2.2.7. Cenozoic

[28] Paleocene deposits are absent in the northern Morondava basin, but as much as ~750 m of limestones, dolomites and marls are preserved in the southern and central Morondava basin [*Coffin and Rabinowitz*, 1988]. The Eocene is composed of a 400–450 m thick marine carbonate sequence in the south, which looses its marine character to the north and thins to 10–15 m [*Coffin and Rabinowitz*, 1988]. In the northern part of the basin no Oligocene deposits are present, while in the south there are about 400 m of marls [*Coffin and Rabinowitz*, 1988]. During the Miocene, up to 275 m of carbonate rocks were deposited in the northern and southern Morondava basin [*Coffin and Rabinowitz*, 1988] and volcanics, dated by the K-Ar method at 8.9–9.4 Ma, are present in the southern Morondava basin [*Rasamimanana et al.*, 1998; *Bardintzeff et al.*, 2010]. Sedimentation of red continental sandstones in the coastal lowlands reached a thickness of 50 to 100 m during the Pliocene and is continuing until the present [*Coffin and Rabinowitz*, 1988].

3. Fission Track

3.1. Previous Fission Track Data From Central and Southern Madagascar

[29] *Seward et al.* [2004] summarize and interpret previous results covering the whole crystalline basement of Madagascar. The spatial distribution of apparent AFT ages between 431 Ma and 68 Ma and zircon FT ages between 452 and 238 Ma allows for a division of the basement into three major domains from north to south with distinguishable low-temperature evolutions [*Seward et al.*, 2004, Figure 5]. Each of these domains can be subdivided into an eastern and western domain, respectively. Whereas the northern domain shows a diffuse transition to the central domain, which contains the oldest apparent AFT ages, the separation between the central and southern domain is characterized by a significant jump in ages across the NW-SE trending brittle faults within the Ranotsara zone. Furthermore, thermal modeling of the western basement region indicates that initial Paleozoic exhumation was followed by heating (interpreted as burial) during Jurassic to Tertiary times. *Seward et al.* [2004] discuss the eastern limit of sedimentation on the basement as the result of a marine transgression on the western passive margin to be as far east as approximately the Andringitra massif in the south - and almost to the Ankaratra massif in central Madagascar.

[30] *Emmel et al.* [2004, 2006a] present AFT ages between 460 and 79 Ma, as well as titanite FT ages between 483 and 266 Ma. Based on combined apatite and titanite FT data from the central region of Madagascar, they suggest that final cooling after the Late Neoproterozoic/Cambrian metamorphic overprint terminated at ~500 Ma and was followed by a phase of minor cooling related to tectonic quiescence and isostatic compensation lasting until the Carboniferous. They infer denudation rates of ~200–100 m Ma^{-1} for the western palaeo-margin of Madagascar and denudation rates of ~110–25 m Ma^{-1} further inland during the Carboniferous followed by burial of sediments up to ~4.5 km thick during Permo-Triassic rifting. Their FT data show no significant influence of the Jurassic break-up. However, their AFT data from southern Madagascar show a thermal overprint attributed to Late Cretaceous and Cenozoic volcanic activity. *Emmel et al.* [2006b] present detrital AFT ages from Middle Jurassic sediments from the southern Morondava basin ranging between 428 and 233 Ma. Based on this data they suggest

erosion and re-sedimentation of Karroo sediments due to the westward shift of the rift locus in Early Jurassic times.

[31] *Emmel et al.* [2008] discuss the geodynamic evolution of the Precambrian Vohibory terrane, which borders the Morondava basin in SW Madagascar. Combining various geochronometers—including U-Pb titanite (SHRIMP) and $^{40}Ar/^{39}Ar$ biotite—with AFT data, they suggest that crustal extension in the Vohibory terrane started in the Late Carboniferous/Early Permian with cooling rates of 5.3°C/Ma between 350 and 300 Ma associated with initiation of brittle faulting. During the Late Permian/Early Triassic, sediments were deposited in the middle of the Vohibory terrane, while its eastern flank had already started to erode. The basement in the center of the terrane was reheated to >110°C during the Late Triassic/Early Jurassic, due to deposition of the Isalo Group. From that time onward, exhumation propagated from east to west.

[32] *Jöns et al.* [2009] using a multithermochronometer approach on basement rocks in northernmost Madagascar determined AFT ages between ~320 and ~160 Ma, with the two oldest ages of ~320 Ma and ~280 Ma being located close to the boundary with the westerly adjacent Diego-Suarez and Mahajanga basin, respectively. Following high-temperature metamorphism at ~515 Ma (U-Th-Pb monazite), the basement rocks cooled from ~280°C to ~60°C during Permian to early Jurassic. The authors attribute this cooling to the rifting and development of a passive margin. Their model suggests constant temperatures of the basement rocks of ~60°C until final exhumation to the surface commenced in early Miocene.

3.2. Fission Track Methodology

[33] All samples were processed using standard mechanical techniques (jaw crusher, disk mill, hand-sieves) and apatite separates were concentrated using Wilfley table, heavy liquids and magnetic separator. Etching of the apatite was done with 7% HNO_3, at 21°C for 50 s. This etchant results in track length parameters similar to those obtained at 21°C for 20 s with a 5M HNO_3 [*Seward et al.*, 2000b]. There are no published correction methods for variable etches for length measurements. Since the length measurement errors in the work by *Seward et al.* [2000b] were ±0.6 μm between operators, we conclude that our chosen etch of 7% HNO_3 also calibrates within error of the measurements of 5.5M HNO_3 for 20 s at 21°C, the etch incorporated in the modeling methods used here [*Ketcham*, 2005a]. This point only emphasizes the need for further cross calibration studies and/or more consistency in choosing a consistent etch between laboratories, especially when using the acquired data sets for modeling procedures. Further, for clarity at this point, it must be noted here that length and Dpar etch rates do not have a simple linear relationship and have to be treated separately [*Ravenhurst et al.*, 2003, *Sobel and Seward*, 2010]. AFT ages were completed using the external detector method [*Gleadow*, 1981]. Muscovite, the external detector, was etched in 40% HF for 50 min at room temperature. Samples JG 40 to JG 69 were irradiated at ANSTO facility, Lucas Heights, Australia, whereas samples JGI 171 and JGI 173 were irradiated at Oregon State University TRIGA reactor. No statistical differences in the resulting zeta values were detected. Microscopic analyses were carried out at 1250 times magnification using an optical microscope equipped with a computer driven stage [Software: FT Stage 4.01a, *Dumitru*, 1993] at the ETH Zürich fission track laboratory. Ages were determined using the Zeta calibration method [*Hurford and Green*, 1983] with a zeta value of 329 ± 20 (2σ) for glass CN5 (JG). Trackkey software [*Dunkl*, 2002] was used for AFT data processing. All ages are reported as central ages (Table 1) [*Galbraith and Laslett*, 1993] with 2σ error and are rounded to millions of years. Between 20 and 21 grains were counted and 67 to 125 confined tracks were measured per basement sample and 19 to 33 grains (all possible) were counted for sediment samples (Table 1). Generally an insufficient number of lengths was found in the detrital apatites for modeling procedures.

[34] The chemical composition of the measured apatite grains is an important factor influencing the annealing behavior of the fission tracks [*Gleadow and Duddy*, 1981; *Barbarand et al.*, 2003]. Etch pit diameter (Dpar), which is an accepted proxy for annealing kinetics in apatite [*Burtner et al.*, 1994; *Donelick et al.*, 1999, 2005] was measured for all samples. Such data is incorporated into the modeling program of *Ketcham* [2005a] based on an etch of 5.5 M HNO_3. Our Dpar data were corrected to this etchant [*Sobel and Seward*, 2010]. Annealing of fission tracks in apatite is anisotropic [*Green and Durrani*, 1977] and the shortening rate of the tracks is dependent on their orientation relative to the crystallographic axis [e.g., *Green and Durrani*, 1977; *Galbraith and Laslett*, 1988; *Donelick et al.*, 1999; *Ketcham*, 2003, 2005b; *Ketcham et al.*, 2007a, 2007b]. To eliminate a possible crystallographic biasing of the track lengths statistics, track lengths were projected to a c-axis parallel equivalent. Measured track length data as well as c-axis projected data are presented in Table 1. Unless stated otherwise, track length data throughout the discussion will be c-axis corrected equivalents.

[35] In summary, thermal modeling of basement samples was performed with Hefty beta version 6 software [*Ketcham*, 2005a], c-axis projection after *Donelick et al.* [1999] and annealing model after *Ketcham et al.* [1999] assuming an initial (unannealed) track length as a function of our corrected Dpar values, which are used as the kinetic indicator.

4. Results and Interpretation

[36] The AFT ages of the Proterozoic basement samples in the Malaimbandy and the Iloto area (Figure 1) lie between 217 ± 29 Ma and 332 ± 50 Ma with mean track lengths (MTLs) between 12.72 ± 0.12 μm (SD = 1.32) and 14.35 ± 0.10 μm (SD = 0.9) (Table 1). The central AFT ages of the sediment samples are between 94 ± 20 Ma and 260 ± 36 Ma in age, with MTLs between 13.04 ± 0.15 μm (SD = 1.18) and 14.45 ± 0.16 μm (SD = 0.79) (Table 1).

[37] The MTLs, broad track-length distributions (Table 1) and the non-systematic relation of MTL against AFT age indicate varying thermal histories for the different samples and account for an overall protracted thermal history (Figure 3). All samples from the Malaimbandy area can be considered to have similar annealing kinetics on the basis of average corrected Dpar values between 1.26 μm and 1.47 μm (Figure 3). Apatite with Dpar values ≤1.75 μm (etching with 5.5M HNO_3 for 20 s at 21°C) are most likely fluorapatite [*Donelick*

Table 1. Apatite Fission-Track Data From Sedimentary and Basement Rocks of the Morondava Rift Basin Shoulder

Sample	Latitude, Longitude	Altitude (m)	Rock Type	Counted Grains	$Rho_D \times 10^5 cm^{-2}$ (Counted)[a]	$Rho_S \times 10^5 cm^{-2}$ (Counted)[b]	$Rho_I \times 10^5 cm^{-2}$ (Counted)[b]	U (ppm)	Mean Track Length (SD) (μm)	C-Axis Equivalent MTL (SD)[c] (μm)	Number of Confined Tracks	$P(\chi^2)$[d]	Dispersion[e]	Age $\pm 2\sigma$[f] (Ma)
Karroo Sediments (Malaimbandy)														
JG 46	S 20.50751, E 45.83225	1114	Sandstone/ Conglomerate	19	11.87 (8929)	15.38 (909)	11.38 (673)	14.30	12.89 ± 0.39 (1.99)	14.26 ± 0.22 (1.14)	26	25	0.12	260 ± 36
JG 48	S 20.46725, E 45.79160	848	Quartzitic Sandstone	32	10.86 (8929)	10.09 (458)	7.56 (343)	8.91				<1	0.38	212 ± 36
JGI 171	S 20.39889, E 45.69640	198	Sandstone	33	12.87 (7820)	14.20 (1821)	15.04 (1929)	15.59	11.19 ± 0.27 (2.10)	13.04 ± 0.15 (1.18)	60	<1	0.17	205 ± 25
JGI 173	S 20.37417, E 45.60832	180	Sandstone	33	13.16 (7820)	8.99 (830)	21.58 (1993)	18.56	13.23 ± 0.25 (1.22)	14.45 ± 0.16 (0.79)	24	0	0.45	94 ± 20
Basement (Malaimbandy)														
JG 40	S 20.532933, E 45.93283	1103	Orthogneiss	20	12.21 (8929)	23.24 (1982)	17.35 (1480	18.33	11.73 ± 0.21 (2.15)	13.65 ± 0.11 (1.13)	105	0	0.23	268 ± 39
JG 47	S 20.482533, E 45.81725	1010	Orthogneiss	20	11.60 (8929)	58.92 (1992)	32.33 (1093)	37.02	12.15 ± 0.14 (1.45)	13.62 ± 0.09 (0.94)	107	0	0.24	332 ± 50
JG 49	S 20.466767, E 45.78445	840	Orthogneiss	21	11.06 (8929)	31.74 (3412)	20.17 (2168)	21.34	11.48 ± 0.18 (1.80)	13.12 ± 0.11 (1.16)	105	<1	0.13	288 ± 30
JG 50	S 20.463867, E 45.76358	625	Orthogneiss	20	10.65 (8929)	33.61 (3442)	21.81 (2233)	25.13	10.75 ± 0.17 (1.89)	12.72 ± 0.12 (1.32)	125	14	0.07	265 ± 25
JG 52	S 20.454933, E 45.74786	417	Orthogneiss	20	11.55 (5990)	17.62 (1741)	15.28 (1510)	15.43	11.12 ± 0.16 (1.77)	13.13 ± 0.10 (1.07)	122	0	0.19	217 ± 29
Basement (Iloto)														
JG 68	S 21.995817, E 45.52453	516	Migmatite	20	10.77 (5990)	33.77 (2014)	22.08 (1317)	23.32	13.07 ± 0.15 (1.38)	14.35 ± 0.10 (0.90)	80	<1	0.18	274 ± 36
JG 69	S 21.996467, E 45.52788	651	Qtz-Fsp-Gneiss	20	9.98 (5990)	47.79 (1998)	32.86 (1367)	38.25	12.71 ± 0.21 (1.68)	14.03 ± 0.12 (0.99)	67	0	0.18	250 ± 34

[a] Rho_D represents the standard track density.
[b] Rho_s and Rho_i represent sample spontaneous and induced track densities.
[c] C-axis equivalent track lengths conversion after *Donelick et al.* [1999].
[d] $P(\chi^2)$ probability of passing the chi square test according to *Green* [1981].
[e] Dispersion values from Trackkey software.
[f] Ages are presented as central ages with a 2 sigma error [*Galbraith and Laslett*, 1993]. Zeta = 329 ± 20 for CN5 (JG). Irradiation of samples JG 40 to JG 69 at ANSTO facility, Lucas Heights, Australia, and of samples JGI 171 and JGI 173 at Oregon State University TRIGA reactor.

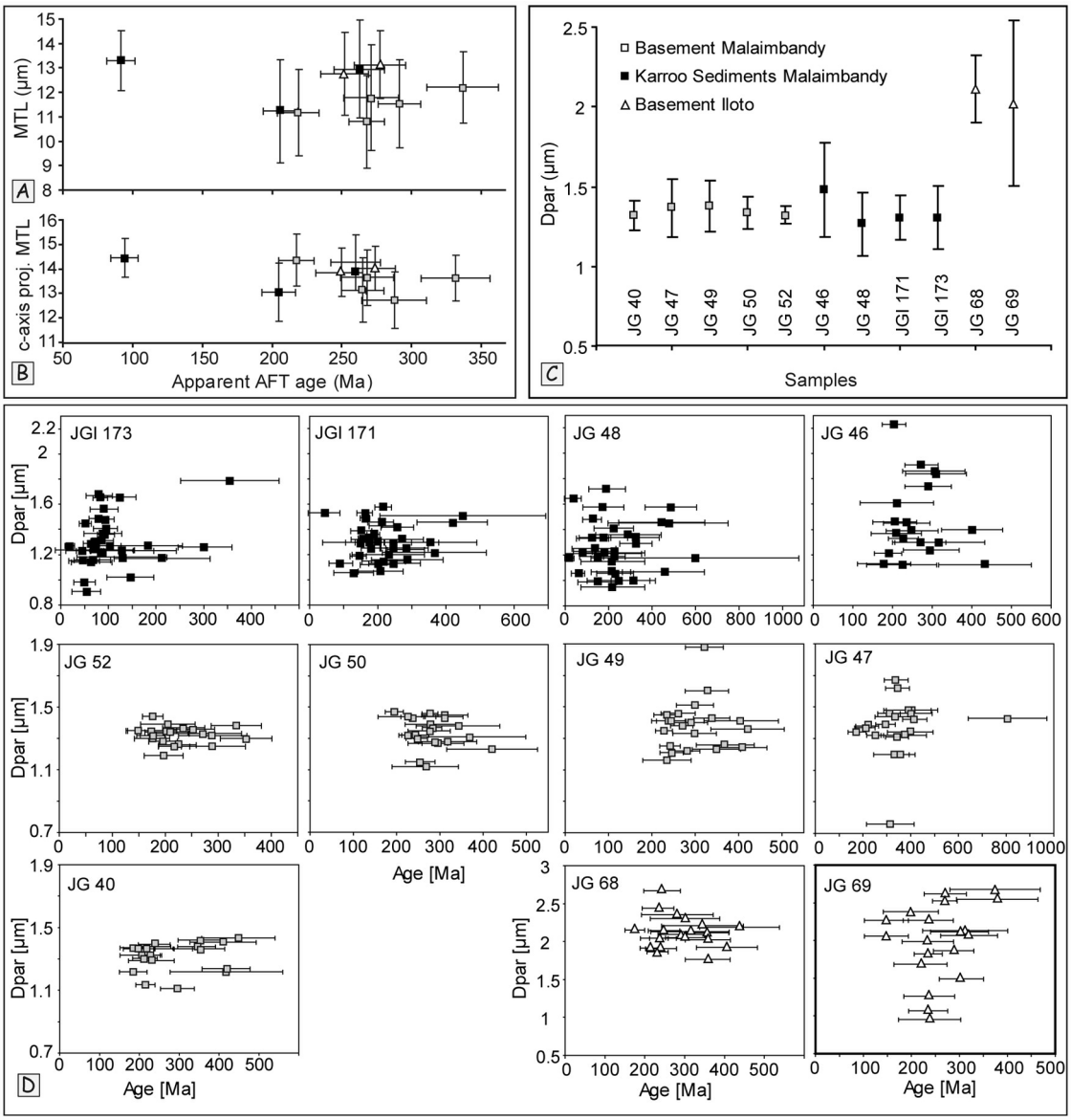

Figure 3. (a and b) Apparent AFT age of samples versus mean track lengths (MTL) and c-axis projected equivalent mean track lengths, respectively. Uncertainties are 2σ for the ages and one standard deviation for the mean track lengths. Dark gray and light gray boxes indicate sediment and basement samples from the Malaimbandy area, respectively; open triangles are basement samples from the Iloto area. (c) Corrected etch pit mean diameter (Dpar) values for apatite samples. Uncertainty given is a 1σ standard deviation for the average grain Dpar (5 measurements per grain). Note the consistent values for the Malaimbandy samples and the difference to the Iloto samples. (d) Single grain AFT ages versus etch pit diameter (Dpar).

et al., 2005, and references therein]. The two samples from the Iloto area have Dpar values of 2.02 μm and 2.12 μm (Figure 3).

4.1. Malaimbandy Area

[38] Across the basin-basement contact, five granitoid orthogneisses (JG 40, JG 47, JG 49, JG 50 and JG 52) and 4 siliciclastic sediment samples (JG 46, JG 48, JGI 171 and JGI 173) were collected along transect Y-Y′ (Figure 4). In the Malaimbandy area, close to the contact with the sediments, the basement rises to more than 1000 m above the sedimentary plain within approximately 10 km of horizontal east to west distance, marking the western edge of the high plateau (Figures 4 and 5). Remnants of Isalo I sediments rest unconformably on basement close to the western edge of the high plateau at altitudes greater than 1000 m (Table 1 and Figure 4), allowing sampling of both basement and sedimentary rocks in a section across the escarpment.

4.1.1. Basement Samples

[39] The oldest apparent AFT age of 332 $\pm$ 50 Ma (JG 47) is obtained on a local topographic crest at an altitude of 1010 m, just east of the major altitude difference of the escarpment (Figures 4 and 5). Downslope, the apparent AFT

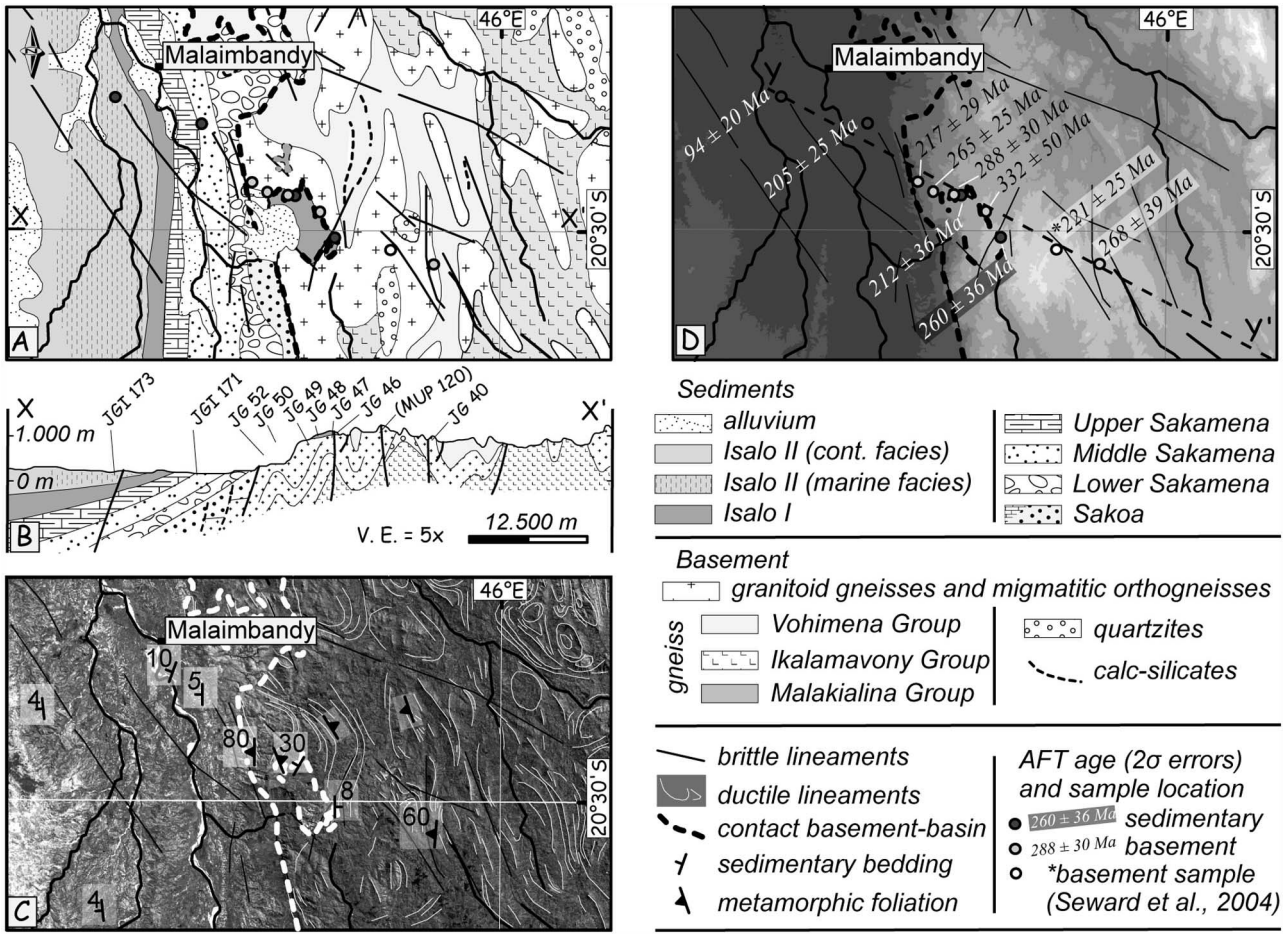

Figure 4. (a) Detailed geological map of the Malaimbandy area (modified after *Bésairie* [1969a]). X-X′ indicates position of geological profile. (b) Schematic geological profile with position of samples. Five times vertical exaggeration. (c) Panchromatic Landsat ETM+ 7 image, spatial resolution 15 by 15 m. (d) Digital elevation model SRTM [*USGS*, 2004]; Y-Y′ indicates position of topographic profile in Figure 5.

ages become progressively younger toward the basin (west), the youngest AFT age from the basement (JG 52, 217 ± 29 Ma) is located close to the sedimentary plain at an altitude of 417 m (Figures 4 and 5). Although four successive basement samples (JG 47, JG 49, JG 50 and JG 52) yield a positive correlation between apparent AFT ages and altitudes (Table 1), the exhumation rate cannot be estimated. Exhumation rates derived only from an age-altitude relationship of AFT data, should be based on vertical sections and on samples representing only one cooling/exhumation event. The apparent AFT age of 217 ± 29 Ma (JG 52) is younger than the stratigraphic age of the nearby sediments of the Lower Sakamena Group (~260–251 Ma) which were at one time presumably overlying this basement. The apparent ages of JG 50 and JG 49, 265 ± 25 Ma and 288 ± 30 Ma respectively, are slightly older than the stratigraphic age (~238–231 Ma) of the overlying sediments of the Isalo I Formation (JG 46 and JG 48). These age constraints, the shortened MTLs and wide track lengths distributions (12.72 μm (SD 1.32) to 13.62 μm (SD 0.94); Table 1), the large scatter of single grain ages and low P(χ^2) probability of these samples (Figure 7 and Table 1) suggest slow cooling and/or partial resetting of the apatites. Post-depositional partial resetting is supported by the modeled thermal evolution (section 3.4)

Figure 5. AFT data and thermal models (time-temperature paths) for the Malaimbandy area. (a) Track-length distribution histograms of horizontal confined tracks. Dark gray columns indicate the measured track lengths distribution, light gray columns indicate the c-axis projected equivalent track-length distribution. C-axis projection after *Donelick et al.* [1999]. Arrows point to significantly shorter track lengths (also in Figure 5e). (b) Radial plots of sedimentary samples, light gray field indicates the stratigraphic age. (c) Topographic profile Y-Y′ indicating locations of samples. Profile with 5 times vertical exaggeration; location is given in Figure 4d. (d) Radial plots of basement samples. (e) Track-length distribution histograms of horizontal confined tracks. (f) Thermal models from forward modeling using HeFTy beta 6 software [*Ketcham*, 2005a] for the basement samples. Areas in light gray indicate acceptable paths, dark gray areas indicate good paths, and dashed lines give the best fit. Stars indicate turning points from heating to cooling for best fit paths. GOF, goodness of fit; A, comparing measured and modeled ages; L, comparing measured and modeled track lengths.

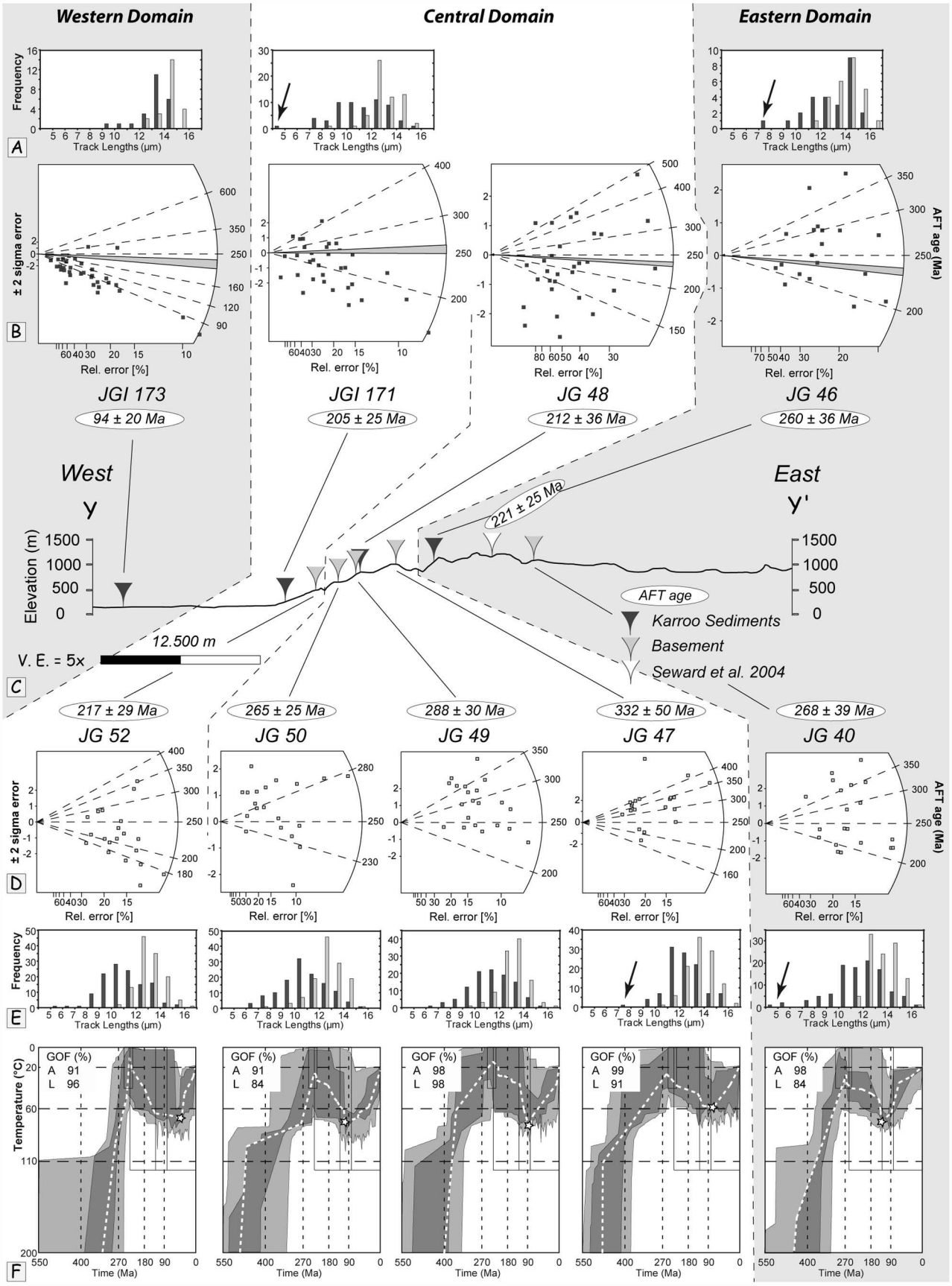
Western Domain
Central Domain
Eastern Domain
Frequency
Track Lengths (µm)
A
± 2 sigma error
Rel. error [%]
AFT age (Ma)
B
JGI 173
94 ± 20 Ma
JGI 171
205 ± 25 Ma
JG 48
212 ± 36 Ma
JG 46
260 ± 36 Ma
West
y
East
y'
221 ± 25 Ma
Elevation (m)
1500
1000
500
0
12.500 m
V. E. = 5x
AFT age
Karroo Sediments
Basement
Seward et al. 2004
C
217 ± 29 Ma
JG 52
265 ± 25 Ma
JG 50
288 ± 30 Ma
JG 49
332 ± 50 Ma
JG 47
268 ± 39 Ma
JG 40
D
E
Temperature (°C)
GOF (%)
A 91
L 96
A 91
L 84
A 98
L 98
A 99
L 91
A 98
L 84
Time (Ma)
F

Figure 5

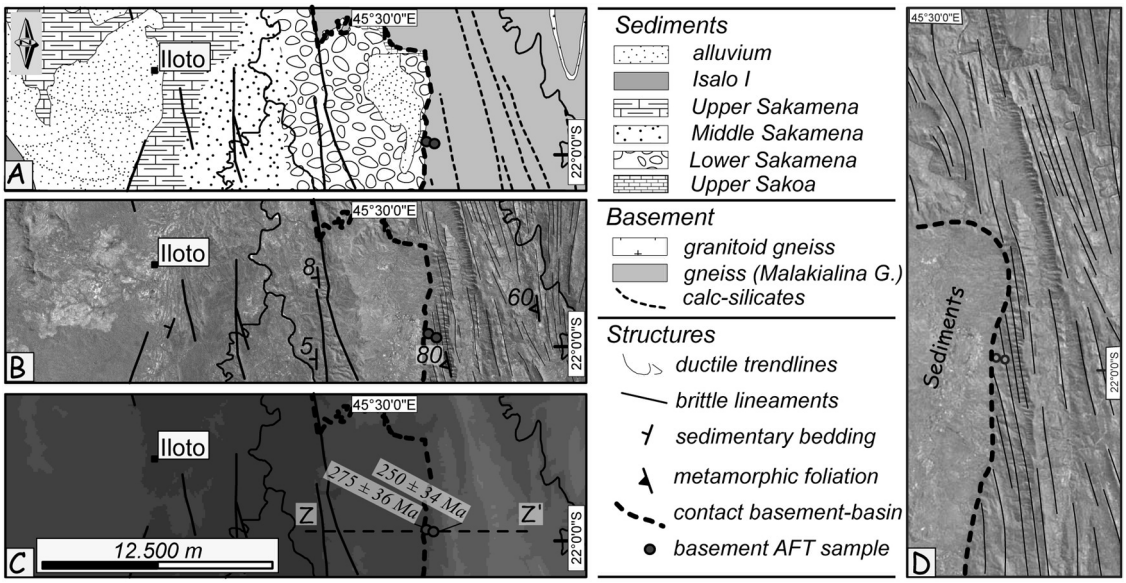

Figure 6. (a) Detailed geological map of the Iloto area (modified after *Bésairie* [1969a]). (b) Panchromatic Landsat ETM+ 7 image, spatial resolution 15 by 15 m. (c) Digital elevation model SRTM [*USGS*, 2004], Z-Z′ indicates position of topographic profile Figure 7. (d) Detail of basement-basin contact, shown on Landsat ETM+ 7 panchromatic image.

which confirms heating of the basement to temperatures greater than 60°C after deposition of the overlying sediments.

[40] The topographically highest basement sample JG 40 at 1103 m yields an apparent AFT age of 268 ± 39 Ma (Table 1) and overlaps in age with basement samples from *Seward et al.* [2004] both further east (MUP 135, 238 ± 22 Ma) and west (MUP 120, 221 ± 25 Ma). MUP 120 is younger than JG 47 (332 ± 50 Ma) to its west (Figure 5). Between these samples, a series of map- to outcrop-scale N-S, NNW-SSE and NNE-SSW striking brittle faults can be observed (Figure 4), and it is likely, that the young age of sample MUP 120 [*Seward et al.*, 2004] is located on the crest of a local horst, bounded on both sides by normal faults. It implies later movement along these faults. Samples JG 40 and JG 47, JG49, JG50, and JG52 are located in the corresponding grabens, yielding older ages (Figures 4 and 5).

4.1.2. Sediment Samples

[41] Two samples (JG 46 and JG 48) are from the Isalo I Group (Figure 2) deposited during the Middle Triassic [after *Hankel*, 1994] from different altitudes (1114 m and 848 m, respectively). JGI 171 is from the Middle Sakamena Group (Early Triassic) at 198 m and JGI 173 belongs to the continental Isalo II Group (Late Triassic) at 180 m (Figures 2 and 4). The AFT ages of these samples become progressively younger from 260 ± 36 Ma in the east to 94 ± 20 Ma in the west, indicating increasing resetting of the apatites independent of the stratigraphic age of the sample. This may be best reflected by the single grain ages: 9 of 19 single grain ages from JG 46 are the same age or younger than the stratigraphic age, indicating partial annealing of the detrital apatite after deposition of the sediment. The degree of annealing becomes stronger toward the west with JG 48 containing 23 of 32 grains younger than the stratigraphic age, JGI 171 with 25 of 33, and finally JGI 173 reaching a maximum of 31 of 33 grains yielding a younger AFT age than the stratigraphic age. The latter sample is thus closer to a complete resetting.

4.2. Iloto Area

[42] The apparent AFT age of a gneiss (JG 69) from the Iloto area (Figure 1) is 250 ± 34 Ma with a MTL of 14.03 μm (SD of 0.99 μm). A nearby migmatite (JG 68) yields an AFT age of 274 ± 36 Ma with a MTL of 14.35 μm (SD of 0.9 μm) (Figures 3, 6, and 7 and Table 1). Both samples feature longer mean track lengths with relatively smaller standard deviations than the basement samples from the Malaimbandy area, which could be an effect of the apparently higher chlorine content indicated by the larger mean Dpar values (Figure 3 and Table 1).

4.3. Thermal History

[43] For each model, the stratigraphic age of the nearest interpolated overlying sediment was chosen as one constraint with the temperatures in the range of 20 ± 20°C. Additional to this, two large boxes of similar dimensions used by *Seward et al.* [2004] and one initial box at metamorphic conditions (500 ± 50 Ma; 500 ± 50°C) were chosen to allow for cooling and heating over a time period of ~550 Ma (Figure 8a), the time since all basement units were amalgamated during the East African Orogen [after *Stern*, 1994]. The end point is constrained to 20°C which is close to median annual temperatures of Madagascar in recent times. The constraints are chosen conservatively in order to provide the models as much freedom as possible. Even so, initial test runs of models showed that acceptable and comparable time-temperature solutions are achieved using (a) slightly different broad constraints, and (b) for repeat runs of samples passing and/or failing the χ^2 test (Figure 8).

[44] The basement samples were at or near to the surface during Late Permian to Middle Triassic times when

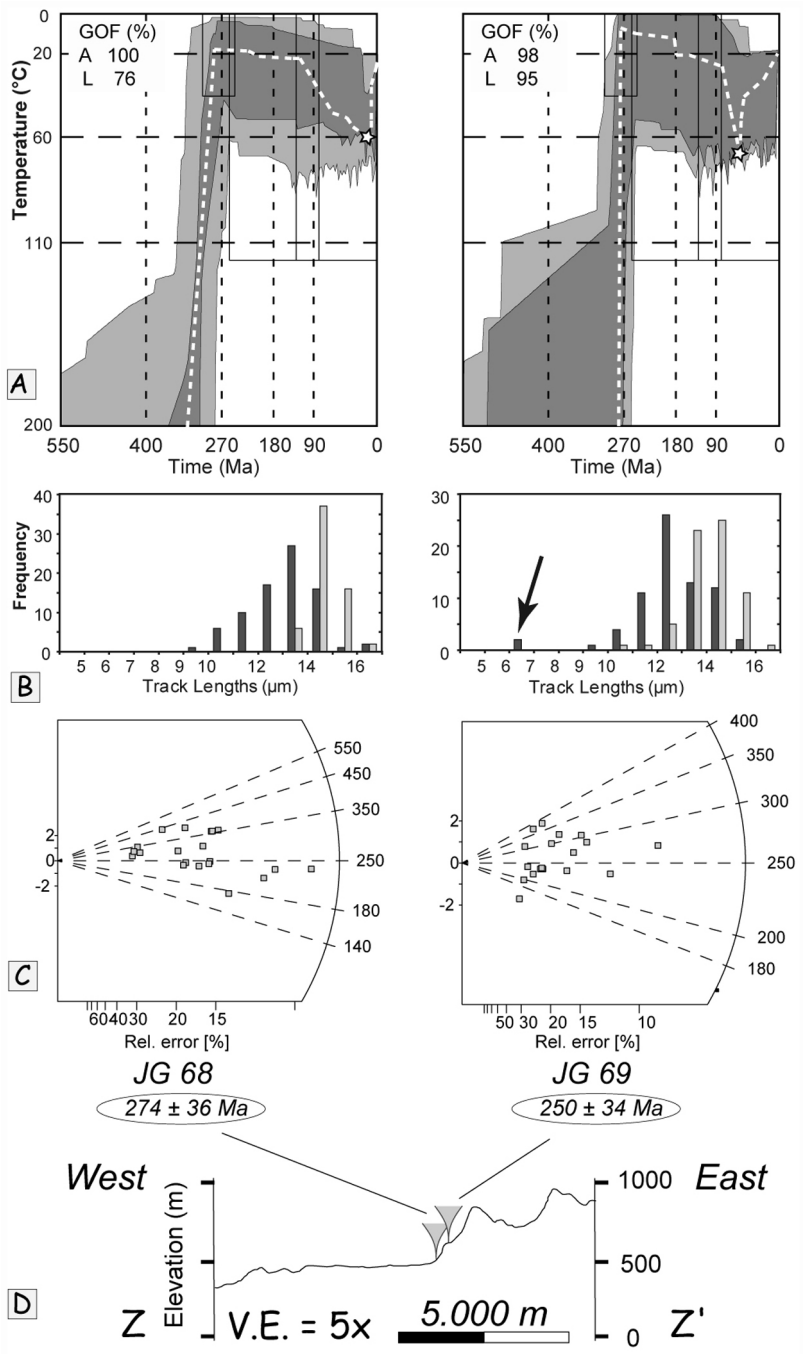

Figure 7. AFT data and thermal models (time-temperature paths) for the Iloto area. (a) Thermal models. (b) Track-length distribution histogram of horizontal confined tracks. (c) Radial plots of analyzed samples. Color coding of 7A and 7B is analogous to Figure 5. (d) Topographic profile Z-Z′ indicating locations of samples. Profile is 5 times vertical exaggerated; location is given in Figure 6c.

sediments of the Sakamena and Isalo I Groups were deposited directly on top. Little confidence can be made in the modeled exhumation patterns leading to that first Palaeozoic to Mesozoic basement surface exposure. The general decrease in apparent AFT ages toward the west and modeled time-temperature paths of all basement samples confirm reheating of the uplifted Morondava rift shoulder to temperatures >60°C before final exhumation (Figure 5). Reheating to temperatures >60°C is also confirmed by the partial resetting of the sediments. The best fit time-temperature paths of the basement rocks reveal significant differences in turning points in the thermal models during the Mesozoic reheating event. Based on the structural position within the former rift shoulder (sedimentary plain, escarpment, rift shoulder), the trend in apparent AFT ages and the partial to almost fully resetting of sediment samples, the transect in the Malaimbandy area can be subdivided into three domains of comparable thermal evolutions, a western (sample JGI

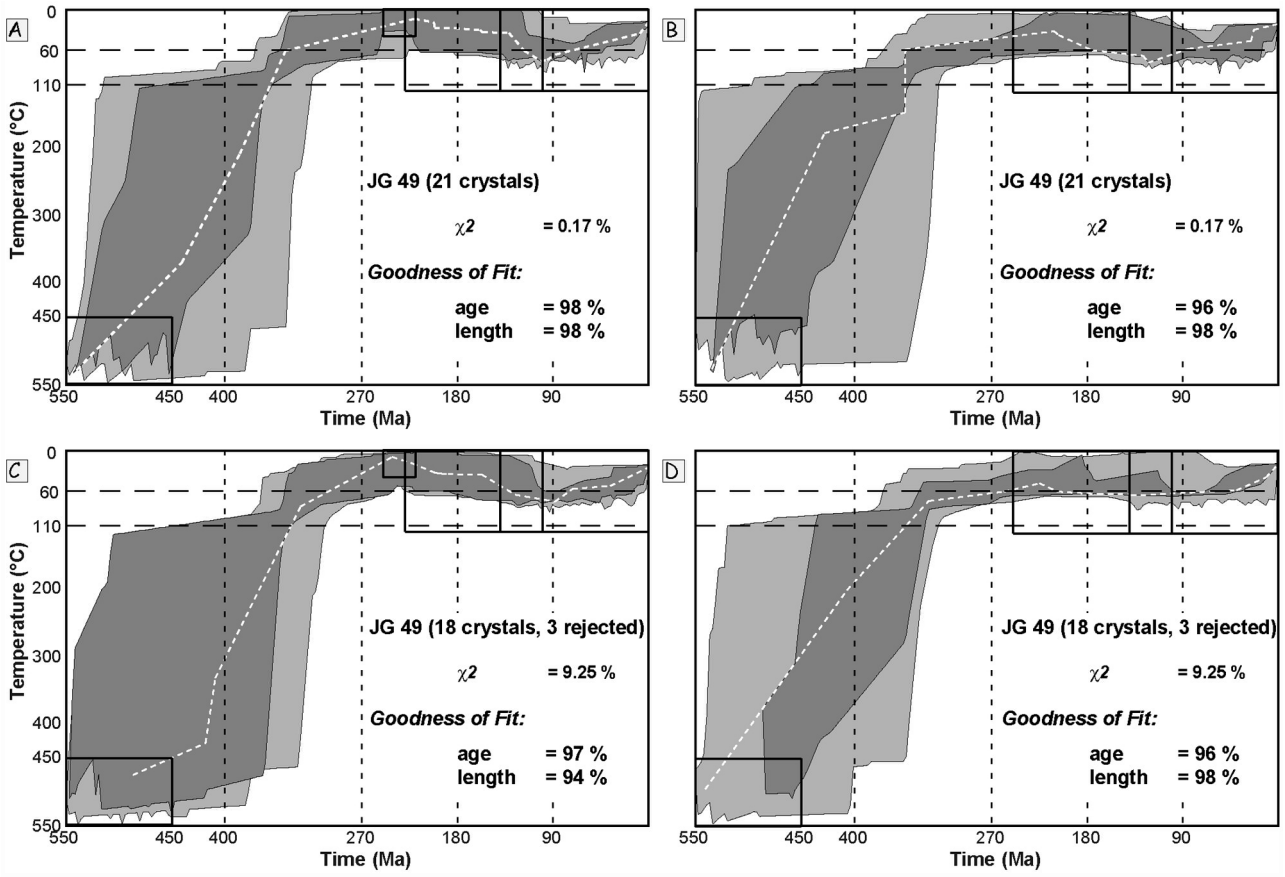

Figure 8. (a–d) Thermal models of sample JG 49 illustrating similar general patterns of time-temperature paths independent from constraints used and χ^2 value of the sample. In all models the best fit solution cools from metamorphic temperatures in Cambrian times to <60°C in late Paleozoic/early Mesozoic times before experiencing reheating to >60°C during the Mesozoic. For all models large constraint boxes at 70 ± 70 Ma and 165 ± 65 Ma, each at 60 ± 60°C and one metamorphic constraint box at 500 ± 50 Ma and 500 ± 50°C was used. Figures 8a and 8c have an additional constraint box representing the stratigraphic age of overlying sediments (Isalo I; 235 ± 15 Ma; 20 ± 20°C). Modeling for Figures 8a and 8b was performed using all single AFT ages with χ^2 probability of 0.17%, and for Figures 8c and 8d the three oldest grains were rejected as outliers, resulting in χ^2 probability of 9.25%. Color coded according to Figure 5f.

173), central (samples JG 47, JG 48, JG 49, JG 50, JG 52 and JGI 171) and eastern domain (samples JG 40 and JG 46; Figure 5), corresponding to the sedimentary plain, the rise of the escarpment, and the basin shoulder, respectively the western edge of the high-plateau. Considering the best fit solution turning points from reheating to cooling are, from east to west, at ~120 Ma (sample JG 40), ~90 Ma (samples JG 47, JG 49 and JG 50), and at ~45 Ma (sample JG 52).

[45] The samples from the Iloto area (Figures 1 and 6) were also reheated to temperatures around or slightly higher than 60°C during the late Jurassic. The transition from heating to cooling for the Iloto area is not well defined by the thermal models (Figure 7).

5. Discussion

[46] AFT data from both sediments and crystalline basement provide information on the evolution of the Morondava basin after deposition of the Late Permian Sakamena and Middle Triassic to Early Jurassic Isalo Group. The initiation of the Morondava basin is marked by deposition of the Late Carboniferous to Early Permian Sakoa Group [*Wescott and Diggens*, 1997]. According to *Schandelmeier et al.* [2004] the deposits of the Sakoa Group, which are found in the southern Morondava basin, are restricted to local pull-apart basins. The Sakoa Group and the basement suffered major erosion, and thus exhumation occurred prior to deposition of the Sakamena Group [e.g., *Coffin and Rabinowitz*, 1988; *Emmel et al.*, 2004]. The latter sediments rest with an angular unconformity on either basement or Sakoa deposits [*Razafimbelo*, 1987; *Coffin and Rabinowitz*, 1988]. However, the 1/500.000 geological map of *Bésairie* [1969a] marks the basement-basin contact east of Iloto as a brittle, approximately N-S trending fault. The 1/100,000 geological maps of this area [*Rakotonanahary et al.*, 1968; *Randriamanantena et al.*, 1967] are contradictory about the nature of this boundary. The interpretation of satellite images shows that the NNW-SSE trending ductile lineaments within the Proterozoic basement east of Iloto strike at a low

angle to the contact with the sediments (Figure 6d) and suggest onlap of Sakamena Group sediments onto the basement.

[47] Further west, within the deposits of the Sakamena Group a series of predominantly NNW-SSE striking brittle faults can be identified on satellite images and in the field (Figure 6). These structures are similarly oriented to ductile trends in the basement to the east and therefore are most likely inherited from the underlying basement. Such reactivation of ductile structures by brittle deformation has been proposed and described for various locations within the Morondava basin [e.g., *Montenat et al.*, 1993; 1996; *Piqué et al.*, 1999a; *Emmel et al.*, 2004; *Schandelmeier et al.*, 2004].

[48] An AFT signal related to the pre-Sakamena history might be present in the very short track lengths between 4 and $\sim$8 μm (not c-axis corrected values) from basement samples JG 40, JG 47, JG 69 and from sediment samples JG 46 and JGI 171, respectively (Figures 5a, 5e, and 7b, indicated by arrows). After deposition of Middle Sakamena and Isalo I sediments onto the basement in the Malaimbandy area and deposition of Lower Sakamena sediments discordantly onto the basement in the Iloto area both basement and overlying sediments share a common evolution with heating followed by final cooling as the rocks were brought to the surface.

5.1. Reheating and Partial Resetting

[49] Heating of sediments and reheating of underlying basement rocks are usually interpreted to be caused by burial due to sedimentation [e.g., *Seward et al.*, 2004; *Emmel et al.*, 2004, 2006a]. Thermal modeling of the AFT data provides an estimate of the amount of heating or reheating experienced by a sample, and hence serves as a basis for the assumed depth of burial. However, the conversion from temperature to depth requires reliable knowledge about the temporal and spatial evolution of the palaeo-geothermal gradient, which is influenced by heat advection [e.g., *Brown and Summerfield*, 1997], heterogeneous heat production, differing heat conductivities [*Pollack et al.*, 1993] and isotherm distortion related to topographic effects [e.g., *Stüwe et al.*, 1994; *Stüwe and Hintermüller*, 2000]. Despite our lack of knowledge of the palaeo-geothermal conditions, the similarities in single grain age distributions from basement and sediments suggest that thermal conditions were comparable in both rock types on either side of the basement-sediment interface (Figure 5). Formerly proposed long-term palaeo-geothermal gradients range from 20°C/km [*Seward et al.*, 2004] to 30°C/km [*Emmel et al.*, 2004] for the basement of Madagascar and from 34°C to 65°C for sediments in the Morondava basin [*Uhmann*, 1996; *Emmel et al.*, 2006b, 2008]. Therefore, the following estimates about burial depths take into account a minimum uniform geothermal gradient of 20°C/km and a maximum one of 65°C/km.

[50] The heating to temperatures greater than 60°C of the eastern and central domain of the Morondava basin in Late Triassic to Jurassic times most likely starts with the deposition of the Isalo Group. This suggests burial, which is constrained by the depositional age (Isalo I) of JG 46 and JG 48, and confirms the reported thickness of the Isalo Group sequence to exceed 1700 m (up to 6000 m in the south) [*Coffin and Rabinowitz*, 1988]. According to *Schandelmeier et al.* [2004] NNE-SSW and NNW-SSE normal faulting in the Morondava basin exclusively affected Middle Sakamena (Early Triassic) and younger sediments, with faulting mainly restricted during deposition of the Isalo I, a sequence of, in this case, $\sim$1 to 3 km of clastic sediments related to the Karroo rift phase.

[51] In northernmost Madagascar, burial and reheating of basement rocks adjacent to the Mahajanga basin did not occur during Karroo rifting [*Jöns et al.*, 2009]; here the basement experienced monotonous cooling with maximum exhumation from Permo-Triassic until early Jurassic, followed by an episode of constant temperatures of $\sim$60°C until Neogene times.

[52] In the Morondava basin, the initial Karroo rift failed in early Jurassic times and the rift locus shifted westward [*Clark*, 1998; *Geiger et al.*, 2004]. Further to the south and to the north in the Morondava basin exhumation started, according to *Emmel et al.* [2006a, 2006b], during the Jurassic. Our data set does not display this phase of exhumation, but rather indicates a continuation of burial and/or steady state. The comparison to models by *Emmel et al.* [2004, 2006a], however, has to be treated with caution. These authors used both different etching and modeling techniques to those we present here. Such discrepancies only further emphasize the need for more standardization.

[53] The rocks of the Karroo super-group hosted the newly initiated rift [*Montenat et al.*, 1996] and post-Karroo sediments from the late Early Jurassic and younger were deposited over the newly initiated rift shoulder to the east [e.g., *Clark*, 1998]. This most likely resulted in peak temperatures of more than 60°C in the Cretaceous (considering the best fit paths) (Figure 5). It is assumed that this burial does not exclusively relate to the post-Karroo sequences, but is caused by the addition of Karroo and post-Karroo sedimentation.

[54] The westernmost sample, situated about 12 km west from the base of today's escarpment, experienced the highest post-depositional temperatures. On the basis of its nearly complete resetting, peak temperatures of the order of 90–100°C may be assumed. The apparent AFT age of 94 $\pm$ 20 Ma might either be caused by (1) heating associated with Late Cretaceous volcanism, or (2) burial of sediment to depths of $\sim$2 to 5 km (Table 1). Although a thermal impact from nearby basaltic dikes or related heat production cannot be excluded, burial as an agent for the overprint is considered to be more likely. The strongest argument for burial is the overall trend of increasing resetting of detrital single grain ages from east to west (Figure 5). The westward increase in depth of burial over today's basement-basin contact—based on the increase in partial annealing of the sediments—indicates that faulting along the present boundary between basement and sediments occurred during Karroo sedimentation. Estimated denudation rates of the basement derived from fission track data from central and southern Madagascar [*Emmel et al.*, 2004] and sedimentological and structural investigations [e.g., *Razafimbelo*, 1987; *Montenat et al.*, 1996; *Piqué et al.*, 1999a] lead to the interpretation that the basement-basin contact represented an escarpment, produced by syn-sedimentary faulting during Karroo times. Sedimentary rocks, such as those represented by sample JGI 173 clearly attained temperatures characteristic for the oil window. The Morondava basin was formerly, and is at present explored for hydrocarbons. The interest in hydrocarbon potential of Madagascar started in the early 1900s, at a time

when the largest tar sand and heavy oil fields at Bemolanga and Tsimiroro in the NW Morondava basin were discovered [*Clark*, 1998]. Numerous other surface oil impregnations of minor extent are recognized along the eastern, faulted margin of the Morondava basin, but only a few wells have recovered significant quantities of hydrocarbons [*Jeans and van Meerbeke*, 1995]. Although the principal source rock of the Karroo failed rift sequence is thought to be in the Middle Sakamena Group [*Clark*, 1998], source rocks of minor extent and from different stratigraphic levels have been identified [*Jeans and van Meerbeke*, 1995]. Furthermore, rocks from the Sakoa and lower Isalo II groups have been detected as locally significant gas-prone source rocks [*Jeans and van Meerbeke*, 1995]. Oil maturity was probably reached in Late Jurassic or Early Cretaceous times and locally achieved gas maturity in middle Cretaceous times [*Clark*, 1998]. The above considerations match with the almost completely reset sample JGI 173 at ~90 Ma, its stratigraphic age and its structural position at the base of the Karroo basin rift shoulder and support its evolution related to burial rather than thermal overprint by Cretaceous volcanism.

5.2. Final Exhumation

[55] The apparent AFT ages of the basement samples range from 217 ± 29 Ma to 332 ± 50 Ma and are broadly overlapping with AFT ages of fluorapatites from the western basement area (~20°S, less than ~100 km distance to Morondava basin) from *Seward et al.* [2004] (169 ± 18 Ma (M 124) to 339 ± 85 Ma (MUP 103)). Thermal models by *Seward et al.* [2004] indicate reheating during the Mesozoic that lasted until middle Tertiary and is followed by cooling. Heating was suggested to be associated with burial by passive margin sediments. The best fit paths of our thermal models indicate no cooling before ~120 Ma (Early Cretaceous) for the eastern domain and onset of cooling for samples from the central and western domain between ~90–80 Ma (Late Cretaceous) and around ~50–40 Ma (Eocene) in the Malaimbandy area (Figure 5).

[56] The onset of cooling, related to final exhumation clearly postdates seafloor spreading (starting ~165 Ma) within the Mozambique and Somali basins [*Rabinowitz et al.*, 1983] and there is no signal in the AFT ages and thermal models (Figure 5) related to the Jurassic rift which resulted in the break-up between Madagascar and eastern Africa during the Middle Jurassic [*Montenat et al.*, 1996; *Coffin and Rabinowitz*, 1988; *Geiger et al.*, 2004; *Rabinowitz and Woods*, 2006]. This is in agreement with FT data further south [*Emmel et al.*, 2004] that are also not affected by the Jurassic break-up and drift of Madagascar.

[57] Our present data set suggests up to three periods for the onset of cooling, here interpreted as exhumation, during (1) Early Cretaceous, (2) Late Cretaceous, and (3) Eocene times, although there is no strong reason to assume that they could not be perhaps regionally time transgressive.

5.2.1. Early Cretaceous Exhumation

[58] The eastern domain (JG 40) began to cool at ~120 Ma (Figure 5f) which coincides with the proposed end of the relative southward displacement of Madagascar along the Davie Ridge [*Coffin and Rabinowitz*, 1988; *Montenat et al.*, 1993, 1996; *Piqué*, 1999; *Rabinowitz and Woods*, 2006; *Ali and Aitchison*, 2008]. Spreading in the Somali Basin ceased and was taken over by spreading between Madagascar-India and Australia-Antarctica [*Janssen et al.*, 1995]. India performed a slight clockwise rotation away from Madagascar before separating from Australia-Antarctica resulting in transtensional rifting between Madagascar and India [*Reeves and de Wit*, 2000]. Previously belonging to the Madagascar-India-Australia-Antarctica plate, India-Madagascar was again part of the African plate [*Reeves and de Wit*, 2000]. Furthermore, at about 120 Ma the proposed focal point of the Marion hot spot is assumed to have been located beneath the central east coast of Madagascar (Figure 1) [*Torsvik et al.*, 1998].

[59] The Late Jurassic sedimentary sequences, with major phases of non-deposition, decrease dramatically in thickness from south to north and were later affected by predominantly NNW-SSE oriented faults close to the Jurassic-Cretaceous boundary and during Early Cretaceous [*Montenat et al.*, 1996] with displacements of up to several hundred meters [*Montenat et al.*, 1996]. The Early Cretaceous onset of exhumation seems to be guided by these faults, with extension possibly related to either regional thermal doming linked to asthenospheric bulging of the juvenile Marion hot spot or to transtensional rifting caused by rotation of India relative to Madagascar reactivating pre-existing, suitably oriented border faults of the Morondava basin.

[60] The very old apparent AFT ages (e.g., M168, 396 ± 44 Ma; M174, 431 ± 46 Ma) reported by *Seward et al.* [2004] for the central east coast of Madagascar, however, contradict the hypothesis of thermal doming caused by the Marion hot spot at ~120 Ma and we consider that reactivation of structures in the Morondava basin by widespread, diffuse transtensional rifting related to a slight clockwise rotation of India from Madagascar is more plausible for explaining the Early Cretaceous exhumation.

[61] The eastern domain of the Malaimbandy area is located in the "footwall" being subject to an earlier period of exhumation than the region further west (Figures 4 and 5). The subsequent clastic successions of Albian and Cenomanian age are deposited above a noticeable unconformity, partly covering the above mentioned faults [*Montenat et al.*, 1996]. This unconformity and associated erosion are related to uplift [*Luger et al.*, 1994; *Montenat et al.*, 1996]. Motion along normal listric faults ceased after Albian to Cenomanian times [*Piqué*, 1999].

5.2.2. Late Cretaceous Exhumation

[62] At about 90 to 85 Ma, contemporaneous with the break-up between Madagascar and India-Seychelles [e.g., *Rabinowitz and Woods*, 2006], numerous basaltic dikes intruded the Morondava basin with a preferred ENE-WSW and NW-SE orientation. The dikes are most probably related to the coeval activity of the Marion hot spot, whose focal point is assumed to be located at the Volcan de l'Androy in southern Madagascar at that time [*Storey et al.*, 1995]. Asthenospheric upwelling in the Late Cretaceous linked to the Marion hot spot might have caused regional uplift associated with lithospheric thinning. Regional scale doming however contradicts the hypothesis that the whole island of Madagascar formed a flat and near sea level large igneous province in the Late Cretaceous [*de Wit*, 2003, and references therein].

[63] The basaltic dikes cut through the NNW-SSE striking structures [e.g., *Montenat et al.*, 1993] and their placement is coeval or slightly pre-dates the onset of exhumation of the

majority of samples along the central domain of the Malaimbandy transect (Figure 5). Therefore it is likely, that cooling and/or exhumation that started in Late Cretaceous times is related to either (block?) movements along these NW-SE oriented structures parallel to the basaltic dikes, probably reactivated by thermal doming of the Marion hot spot, or perhaps to an adjustment of the geothermal gradient following the major phase of Late Cretaceous magmatism. *Emmel et al.* [2006a] propose for the Miandrivazo area further north, that NW-SE structures were repeatedly activated and hosted a Jurassic phase of exhumation.

5.2.3. Eocene Exhumation

[64] The probable late onset of exhumation in Eocene times between ~40–50 Ma is recognized in the western part of the central domain (JG 52), in large regions east of the study area [*Seward et al.*, 2004], and in the Vohibory region of southern Madagascar [*Emmel et al.*, 2008]. In the latter case, the authors suggest that exhumation was due to isostatic compensation related to the deposition of the Mahafaly carbonate platform of Eocene age in SW Madagascar. Present outcrop suggests that the Eocene sediments rapidly thin out toward the north, where, according to *Coffin and Rabinowitz* [1988] they attain only 10–15 m in thickness and loose their marine character. A similar scenario of isostatic compensation can therefore be excluded for the Eocene onset of exhumation in the central Morondava basin. However, numerous indications such as AFT data in several locations in western Madagascar, the evolution of the Tertiary sedimentary succession in the Morondava basin, as well as accelerated cooling in late Eocene/early Oligocene times in the crystalline basement of eastern Tanzania [*Noble et al.*, 1997] suggest a regional or supra-regional cause for Eocene exhumation. Major unconformities are present in, above and below the Eocene deposits [*Coffin and Rabinowitz*, 1988]. Paleocene deposits thin out toward the north and are absent in the northern Morondava basin, probably eroded due to uplift. *Coffin and Rabinowitz* [1988] report from well data that Eocene sequences unconformably overlie Late Cretaceous deposits offshore in the northern Morondava basin. Additionally, Oligocene deposits are absent in the northern Morondava basin [*Coffin and Rabinowitz*, 1988] and the subsequent Miocene deposits are restricted to small embayments in the southern and northern Morondava basin [*Coffin and Rabinowitz*, 1988]. The Paleogene to Neogene depositional history indicates that the northern and central parts of the Morondava basin—with respect to the southern part—developed as a local high at least since the Eocene. The northern Morondava basin remained a local high until the Miocene.

[65] At ~50 Ma the sub-continent of India collided with Asia and motion along the 90 East Ridge ceased [*Janssen et al.*, 1995, and references therein]. Subsequently, at ~43 Ma a hiatus in plate motion, affecting the whole Indian Ocean was followed by a reorganization of the spreading systems [*Reeves and de Wit*, 2000]. The direction of spreading changed from NE-SW between Madagascar and India, and Antarctica and India, respectively before ~43 Ma to N-S between Madagascar and Antarctica after ~43 Ma [*Reeves and de Wit*, 2000]. This reorientation caused fracturing of the Davie Ridge [*Rabinowitz and Woods*, 2006].

[66] Although, a probable phase of fault activity during the Eocene is not described in Madagascar, predominantly NNE-SSW to NE-SW oriented faults are abundant in Eocene (and younger) sediments along the western coast [*Bésairie*, 1969a; *Piqué*, 1999], providing a maximum age for potential fault activity related to Eocene exhumation. The trigger for the Eocene exhumation might thus be the change in the regional stress field caused by the reorganization of the spreading systems in the Indian Ocean. The newly developed N-S spreading could reactivate NE-SW oriented faults and trigger enhanced subsidence in the southern Morondava basin, which was compensated by relative exhumation in the central and northern Morondava basin and the adjacent western basement regions. To what extent thermal doming of central Madagascar - as a precursor to Miocene to recent volcanism - might have played a role in Eocene exhumation remains enigmatic. A present rise in Moho depth can be inferred from positive Bouguer anomalies beneath the high plateau in central Madagascar [*Fourno and Roussel*, 1994; *Rakotondraompiana et al.*, 1999]. However, there is no consensus about the exact topography of the crust-mantle interface [*Pili et al.*, 1997; *Rakotondraompiana et al.*, 1999] and timing of surface topography development is unknown [*Randiranasolo*, 2009].

6. Conclusions

[67] Thermal signals related to the initial formation of the Morondava basin and the deposition of the Sakoa Group sediments are difficult to reconstruct from fission tracks in apatite of the basement units close to the basement-basin contact.

[68] However, the basement was exposed to, or near the surface during deposition of the overlying Late Permian to Early Jurassic Sakamena and Isalo Groups (Karroo rift) and experienced subsequent thermal overprinting and partial resetting of fission tracks in apatite. All basement samples are partially reset; the apparent AFT age of 217 ± 29 Ma of one basement sample (JG 52) is even slightly younger than the depositional age of the closest, overlying sediment (Middle Sakamena, Early Triassic).

[69] Best fit time-temperature paths suggest maximum temperatures were reached during Mesozoic heating in early and late Cretaceous, as well as in Eocene times. The sediments of the Sakamena and Isalo Groups experienced post-depositional thermal overprint together with the underlying basement. This heating resulted in increasing partial annealing of the fission tracks toward the west, and indicates deeper burial of the Karroo sediments basinward.

[70] Sediments close to the present escarpment (JGI 173) experienced post-depositional temperatures of up to ~90–100°C, which indicates that the Isalo II sediments in this place experienced temperature conditions required for hydrocarbon formation. It further implies that hydrocarbon formation and source rock potential of the Karroo sediments in the Morondava basin might not be restricted to specific stratigraphic levels, but is rather dependent on the structural position and therewith the depth of burial and probable subsequent exhumation respectively.

[71] The increase in amount of partial annealing (burial depths) of the sediment samples toward the west indicates fault activity along the present basement-basin boundary during deposition of the Karroo sediments. The rifting of Madagascar from eastern Africa and the accretion of oceanic

crust in the Somali and Mozambique basins since Middle Jurassic times (~165 Ma) did not yield a clear signal in the AFT data of the Malaimbandy and Iloto areas.

[72] Final cooling of the basin shoulder was initiated in (1) Early Cretaceous (~120 Ma), (2) Late Cretaceous (~80–90 Ma), and (3) Eocene times (~40–50 Ma). All three periods of onset of cooling are considered to be related to exhumation and can be correlated with major changes in plate motions within the Indian Ocean region and indicate a complex cooling history for the entire area. The Early Cretaceous exhumation is a response to diffuse transtensional rifting related to the separation of India from Madagascar while the Late Cretaceous event is contemporaneous with the break-up between Madagascar and India-Seychelles [e.g., *Rabinowitz and Woods*, 2006]. We suggest that the possible Eocene exhumation may be the result of the change in plate motion at about 43 Ma in the Indian Ocean [*Reeves and de Wit*, 2000].

[73] **Acknowledgments.** Alfons Berger and Edwin Gnos contributed helpful discussions and suggestions during fieldwork and thereafter. The helpful and friendly atmosphere of the ETH Zürich fission track group and their support is highly appreciated. Diane and Terry Seward are greatly thanked for welcoming me (J.G.) in Zürich. The comments of three anonymous reviewers and M. Dazinnies are gratefully acknowledged. This study was financed by the Swiss National Science Foundation credits 200020-105453/1 and 200020-118023/1.

References

Ali, J. R., and J. C. Aitchison (2008), Gondwana to Asia: Plate tectonics, paleogeography and the biological connectivity of the Indian subcontinent from the Middle Jurassic through latest Eocene (166–35 Ma), *Earth Sci. Rev.*, *88*, 145–166, doi:10.1016/j.earscirev.2008.01.007.

Barbarand, J., A. Carter, I. Wood, and T. Hurford (2003), Compositional and structural control of fission-track annealing in apatite, *Chem. Geol.*, *198*, 107–137, doi:10.1016/S0009-2541(02)00424-2.

Bardintzeff, J. M., B. Bonin, and G. Rasamimanana (2001), The Cretaceous Morondava volcanic province (West Madagascar): Mineralogical, petrological and geochemical aspects, *J. Afr. Earth Sci.*, *32*, 299–316, doi:10.1016/S0899-5362(01)90008-9.

Bardintzeff, J. M., J.-P. Liégeois, B. Bonin, H. Bellon, and G. Rasamimanana (2010), Madagascar volcanic provinces linked to the Gondwana break-up: Geochemical and isotopic evidences for contrasting mantle sources, *Gondwana Res.*, *18*, 295–314, doi:10.1016/j.gr.2009.11.010.

Bésairie, H. (1969a), Carte géologique de Madagascar: Morondava, feuille 6, scale 1:500.000, Serv. Geol. de Madagascar, Antananarivo.

Bésairie, H. (1969b), Carte géologique de Madagascar: Tananarive, feuille 5, scale 1:500.000, Serv. Geol. de Madagascar, Antananarivo.

Bésairie, H. (1972a), Cartes géologique de Madagascar: Fianarantsoa, feuille 7, scale 1:500.000, Serv. Geol. de Madagascar, Antananarivo.

Bésairie, H. (1972b), Géologie de Madagascar. I. Les terrains sédimentaires, *Ann. Geol. Madagascar*, *35*, 1–463.

Bésairie, H. (1973), Précis de géologie malgache, *Ann. Geol. Madagascar*, *65*, 93–113.

Boger, S. D., C. A. M. Ferreira, W. Hirdes, B. Schulte, T. Jenett, and R. Dallwig (2009a), Carte géologique de Madagascar 1/500 000, feuille 10–Fianarantsoa (avec notice explicative), Minist. de Energ. et des Mines, Proj. de Gouv. des Ressour. Miner., Antananarivo.

Boger, S. D., C. A. M. Ferreira, W. Hirdes, B. Schulte, T. Jenett, and R. Dallwig (2009b), Carte géologique de Madagascar 1/500 000, feuilles 11–Ampanihy et 12–Tôlanaro (avec notice explicative), Minist. de Energ. et des Mines, Proj. de Gouv. des Ressour. Miner., Antananarivo.

Boger, S. D., et al. (2009c), Carte géologique de Madagascar 1/500 000, feuille 7–Morondava (avec notice explicative), Minist. de Energ. et des Mines, Proj. de Gouv. des Ressour. Miner., Antananarivo.

Bouysse, P., V. Mendel, M. Munschy, and J. Ségoufin (2004), The map of the Indian Ocean: Physiographic and Structural mapping of an ocean, explanatory notes, 6 pp., Comm. for the Geol. Map of the World, Paris.

Bremer, F. (2005), Karoo Rifting im Morondava Becken, Madagaskar: Fazielle Entwicklung, Kinematik und Dynamik eines polyphasen Riftbeckens, PhD thesis, Tech. Univ. Berlin, Berlin.

Brown, R. W., and M. A. Summerfield (1997), Some uncertainties in the derivation of rates of denudation from thermochronologic data, *Earth Surf. Processes Landforms*, *22*, 239–248, doi:10.1002/(SICI)1096-9837(199703)22:3<239::AID-ESP751>3.0.CO;2-B.

Burtner, R. L., A. Nigrini, and R. A. Donelick (1994), Thermochronology of Lower Cretaceous source rocks in the Idaho-Wyoming thrust belt, *AAPG Bull.*, *78*, 1613–1636.

Chand, S., and C. Subrahmanyam (2003), Rifting between India and Madagascar - mechanism and isostasy, *Earth Planet. Sci. Lett.*, *210*, 317–332, doi:10.1016/S0012-821X(03)00094-3.

Clark, D. N. (1998), Review of the exploration potential of Madagascar, *Houston Geol. Soc. Bull.*, *40*, 23–29.

Cochran, J. R. (1988), Somali Basin, Chain Ridge, and origin of the northern Somali Basin gravity and geoid low, *J. Geophys. Res.*, *93*, 11,985–12,008, doi:10.1029/JB093iB10p11985.

Coffin, M. F., and P. D. Rabinowitz (1988), *Evolution of the Conjugate East African-Madagascan Margins and the Western Somali Basin*, *Spec. Pap. Geol. Soc. Am.*, *226*, 78 pp.

Coffin, M. F., and P. D. Rabinowitz (1992), The Mesozoic East African and Madagascan conjugate continental margins; stratigraphy and tectonics, in *Geology and Geophysics of Continental Margins*, *AAPG Mem.*, vol. 53, edited by J. S. Watkins et al., pp. 207–240, Am. Assoc. of Pet. Geol, Tulsa, Okla.

Collins, A. S., and B. F. Windley (2002), The tectonic evolution of central and northern Madagascar and its place in the final assembly of Gondwana, *J. Geol.*, *110*, 325–339, doi:10.1086/339535.

de Wit, M. (2003), Madagascar: Heads it's a continent, tails it's an island, *Annu. Rev. Earth Planet. Sci.*, *31*, 213–248, doi:10.1146/annurev.earth.31.100901.141337.

Donelick, R. A., R. A. Ketcham, and W. D. Carlson (1999), Variability of apatite fission-track annealing kinetics: II. Crystallographic orientation effects, *Am. Mineral.*, *84*, 1224–1234.

Donelick, R. A., P. B. O'Sullivan, and R. A. Ketcham (2005), Apatite Fission-Track Analysis, in *Low-Temperature Thermochronology: Techniques, Interpretations, and Applications*, *Rev. Mineral. Geochem.*, *58*, edited by P. W. Reiners and T. A. Ehlers, pp. 49–94, Mineral. Soc. of Am., Chantilly, Va.

Dumitru, T. A. (1993), A new computer-automated microscope stage system for fission-track analysis, *Nucl. Tracks Radiat. Meas.*, *21*, 575–580, doi:10.1016/1359-0189(93)90198-I.

Dunkl, I. (2002), Trackkey: A Windows program for calculation and graphical presentation of fission track data, *Comput. Geosci.*, *28*, 3–12, doi:10.1016/S0098-3004(01)00024-3.

Eagles, G., and M. König (2008), A model of plate kinematics in Gondwana breakup, *Geophys. J. Int.*, *173*, 703–717, doi:10.1111/j.1365-246X.2008.03753.x.

Emmel, B., J. Jacobs, and T. Razakamanana (2004), Titanite and apatite fission track analyses on basement rocks of central-southern Madagascar: Constraints on exhumation and denudation rates along the eastern rift shoulder of the Morondava basin, *J. Afr. Earth Sci.*, *38*, 343–361, doi:10.1016/j.jafrearsci.2003.10.009.

Emmel, B., J. Jacobs, M. Kastowski, and G. Graser (2006a), Phanerozoic upper crustal tectono-thermal development of basement rocks from central Madagascar: An integrated fission-track and structural study, *Tectonophysics*, *412*, 61–86, doi:10.1016/j.tecto.2005.09.008.

Emmel, B., M. Geiger, and J. Jacobs (2006b), Detrital apatite fission-track ages in Middle Jurassic strata at the rifted margin of W Madagascar - indicator for a protracted resedimentation history, *Sediment. Geol.*, *186*, 27–38, doi:10.1016/j.sedgeo.2005.09.022.

Emmel, B., N. Jöns, A. Kröner, J. Jacobs, J. A. Wartho, V. Schenk, T. Razakamanana, and A. Austegard (2008), From closure of the Mozambique Ocean to Gondwana breakup: New evidence from geochronological data of the Vohibory terrane, southwest Madagascar, *J. Geol.*, *116*, 21–38, doi:10.1086/524121.

Fourno, J. P., and J. Roussel (1994), Imaging of the Moho depth in Madagascar through the inversion of gravity data: Geodynamic implications, *Terra Nova*, *6*, 512–519, doi:10.1111/j.1365-3121.1994.tb00895.x.

Galbraith, R. F., and G. M. Laslett (1988), Some calculations relevant to thermal annealing of fission tracks in apatite, *Proc. R. Soc. London, Ser. A*, *419*, 305–321, doi:10.1098/rspa.1988.0109.

Galbraith, R. F., and G. M. Laslett (1993), Statistical-models for mixed fission-track ages, *Nucl. Tracks Radiat. Meas.*, *21*, 459–470, doi:10.1016/1359-0189(93)90185-C.

Geiger, M., D. N. Clark, and W. Mette (2004), Reappraisal of the timing of the breakup of Gondwana based on sedimentological and seismic evidence from the Morondava Basin, Madagascar, *J. Afr. Earth Sci.*, *38*, 363–381, doi:10.1016/j.jafrearsci.2004.02.003.

Giese, J., A. Berger, G. Schreurs, and E. Gnos (2011), The timing of the tectono-metamorphic evolution at the Neoproterozoic-Phanerozoic boundary in central southern Madagascar, *Precambrian Res.*, *185*, 131–148, doi:10.1016/j.precamres.2011.01.002.

Gleadow, A. J. W. (1981), Fission-track dating methods: What are the real alternatives?, *Nucl. Tracks Radiat. Meas.*, *5*, 3–14.

Gleadow, A. J. W., and I. R. Duddy (1981), A natural long-term track annealing experiment for apatite, *Nucl. Tracks Radiat. Meas.*, *5*, 169–174.

Green, P. F. (1981), A new tool at statistics in fission track dating, *Nucl. Tracks*, *5*, 77–86, doi:10.1016/0191-278X(81)90029-9.

Green, P. F., and S. A. Durrani (1977), Annealing studies of tracks in crystals, *Nucl. Tracks*, *1*, 43–55.

Hankel, O. (1994), Early Permian to Middle Jurassic rifting and sedimentation in East Africa and Madagascar, *Geol. Rundsch.*, *83*, 703–710, doi:10.1007/BF00251069.

Hirtz, P. (1950), Phénomènes glaciaires gondwaniens à Madagascar, *Bull. Soc. Geol. Fr.*, *20*, 91–92.

Hottin, G. (1976), Présentation et essai d'interprétation du Précambrien de Madagascar, *Bull. Bur. Rech. Geol. Min., Sect. 4*, *2*, 117–153.

Hurford, A. J., and P. F. Green (1983), The Zeta-age calibration of fission-track dating, *Isot. Geosci.*, *1*, 285–317.

Janssen, M. E., R. A. Stephenson, and S. Cloetingli (1995), Temporal and spatial correlations between changes in plate motions and the evolution of rifted basins in Africa, *Geol. Soc. Am. Bull.*, *107*, 1317–1332, doi:10.1130/0016-7606(1995)107<1317:TASCBC>2.3.CO;2.

Jeans, P. J. F., and G. L. E. van Meerbeke (1995), Geological evolution and hydrocarbon habitat of the Majunga basin and Karroo corridor, Madagascar, paper presented at South African Geological Society Centennial GeoCongress, S. Afr. Geol. Soc., Johannesburg, South Africa.

Jöns, N., B. Emmel, V. Schenk, and T. Razakamanana (2009), From orogenesis to passive margin–the cooling history of the Bemarivo Belt (N Madagascar), a multi-thermometer approach, *Gondwana Res.*, *16*(1), 72–81, doi:10.1016/j.gr.2009.02.006.

Ketcham, R. A. (2003), Observations on the relationship between crystallographic orientation and biasing in apatite fission-track measurements, *Am. Mineral.*, *88*, 817–829.

Ketcham, R. A. (2005a), Forward and inverse modelling of low-temperature thermochronometry data, Low-Temperature Thermochronology: Techniques, interpretations, and applications, *Rev. Mineral. Geochem.*, *58*, 275–314, doi:10.2138/rmg.2005.58.11.

Ketcham, R. A. (2005b), The role of crystallographic angle in characterizing and modelling apatite fission-track length data, *Radiat. Meas.*, *39*, 595–601, doi:10.1016/j.radmeas.2004.07.008.

Ketcham, R. A., R. A. Donelick, and W. D. Carlson (1999), Variability of apatite fission-track annealing kinetics: III. Extrapolation to geological time scales, *Am. Mineral.*, *84*, 1235–1255.

Ketcham, R. A., A. Carter, R. A. Donelick, J. Barbarand, and A. J. Hurford (2007a), Improved measurement of fission-track annealing in apatite using c-axis projection, *Am. Mineral.*, *92*, 789–798, doi:10.2138/am.2007.2280.

Ketcham, R. A., A. C. Carter, R. A. Donelick, J. Barbarand, and A. J. Hurford (2007b), Improved modeling of fission-track annealing in apatite, *Am. Mineral.*, *92*, 799–810, doi:10.2138/am.2007.2281.

Kusky, T. M., E. Toraman, and T. Raharimahefa (2007), The Great Rift Valley of Madagascar: An extension of the Africa-Somali diffusive plate boundary?, *Gondwana Res.*, *11*, 577–579, doi:10.1016/j.gr.2006.11.009.

Laville, E., A. Piqué, J. C. Plaziat, P. Gioan, R. Rakotomalala, Y. Ravololonirina, and E. Tidahy (1998), Plio-Quaternary and Recent extensional tectonism in the Madagascar high plateaux: The Ankay-Alaotra graben, *Bull. Soc. Geol. Fr.*, *169*, 775–788.

Luger, P., M. Groschke, M. Bussmann, A. Dina, W. Mette, A. Uhmann, and H. Kallenbach (1994), Comparison of the Jurassic and Cretaceous sedimentary cycles of Somalia and Madagascar: Implications for the Gondwana breakup, *Geol. Rundsch.*, *83*, 711–727, doi:10.1007/BF00251070.

Malod, J. A., D. Mougenot, S. Raillard, and A. Maillard (1991), New constraints on the kinematics of Madagascar: Ttectonic structures of the Davie Ridge, *C. R. Acad. Sci., Ser. II*, *312*, 1639–1646.

Martelat, J.-E., J.-M. Lardeaux, C. Nicollet, and R. Rakotondrazafy (2000), Strain pattern and late Precambrian deformation history of southern Madagascar, *Precambrian Res.*, *102*, 1–20, doi:10.1016/S0301-9268(99)00083-2.

Meert, J. G., and E. Tamrat (2006), Paleomagnetic evidence for a stationary Marion hotspot: Additional paleomagnetic data from Madagascar, *Gondwana Res.*, *10*, 340–348, doi:10.1016/j.gr.2006.04.008.

Montenat, C., L. Ramahavory, and M. Croisile (1993), Tectonic-Sedimentary Sequence of the western Malagasy margin during Jurassic times (Morondava Basin, Madagascar), *C. R. Acad. Sci., Ser. II*, *317*, 811–818.

Montenat, C., L. Ramahavory, and M. Croisile (1996), Tectonic and sedimentary evolution of the Western Madagascan margin during the Jurassic in the Morondava basin, Madagascar, *Bull. Cent. Rech. Explor.-Prod. Elf-Aquitaine*, *20*, 323–340.

Mougenot, D., M. Recq, P. Virlogeux, and C. Lepvrier (1986), Seaward extension of the East-African Rift, *Nature*, *321*, 599–603, doi:10.1038/321599a0.

Noble, W. P., D. A. Foster, and A. J. W. Gleadow (1997), The post-Pan-African thermal and extensional history of crystalline basement rocks in eastern Tanzania, *Tectonophysics*, *275*, 331–350, doi:10.1016/S0040-1951(97)00026-7.

Pili, E., S. M. F. Sheppard, J.-M. Lardeauy, J.-E. Martelat, and C. Nicollet (1997), Fluid flow vs. scale of shear zones in the lower continental crust and the granulite paradox, *Geology*, *25*, 15–18, doi:10.1130/0091-7613(1997)025<0015:FFVSOS>2.3.CO;2.

Piqué, A. (1999), The geological evolution of Madagascar: An introduction, *J. Afr. Earth Sci.*, *28*, 919–930.

Piqué, A., E. Laville, G. Bignot, M. Rabarimanana, and C. Thouin (1999a), The initiation and development of the Morondava Basin [Madagascar] from the Late Carboniferous to the Middle Jurassic: Sedimentary, palaeontological and structural data, *J. Afr. Earth Sci.*, *28*, 931–948.

Piqué, A., E. Laville, P. Chotin, J. Chorowicz, S. Rakotondraompiana, and C. Thouin (1999b), Neogene and present extension in Madagascar: Structural and geophysical data, *J. Afr. Earth Sci.*, *28*, 975–983.

Plummer, P. S. (1996), The Amirante ridge/trough complex: Response to rotational transform rift/drift between Seychelles and Madagascar, *Terra Nova*, *8*, 34–47, doi:10.1111/j.1365-3121.1996.tb00723.x.

Pollack, H. N., S. J. Hurter, and J. R. Johnson (1993), Heat flow from the earth's interior: Analysis of the global data set, *Rev. Geophys.*, *31*(3), 267–280, doi:10.1029/93RG01249.

Rabinowitz, P. D., and S. Woods (2006), The Africa-Madagascar connection and mammalian migrations, *J. Afr. Earth Sci.*, *44*, 270–276, doi:10.1016/j.jafrearsci.2005.12.005.

Rabinowitz, P. D., M. F. Coffin, and D. Falvey (1983), The separation of Madagascar and Africa, *Science*, *220*, 67–69, doi:10.1126/science.220.4592.67.

Rakotonanahary, R., A. Rakotomanga, and J. Rakotoarisaina (1968), Carte géologique de Madagascar: Bekisopa, *Map IJ 54*, scale 1:100.000, Serv. Geol. de Madagascar, Antananarivo.

Rakotondraompiana, S. A., Y. Albouy, and A. Piqué (1999), Lithospheric model of the Madagascar island [western Indian Ocean]: A new interpretation of the gravity data, *J. Afr. Earth Sci.*, *28*, 961–973, doi:10.1016/S0899-5362(99)00072-X.

Randiranasolo, E. B. (2009), Nouvelle methodes de cartographie sur le socle proterozoique du sud de Madagascar, PhD thesis, Univ. Joseph Fourrier, Grenoble, France.

Randriamanantena, Z., Rakotondrasoa, and J. D. Randrianarisoa (1967), Carte géologique de Madagascar: Marandra/Satrokala, *Map IJ 55*, scale 1:100.000, Serv. Geol. de Madagascar, Antananarivo.

Rasamimanana, G., J. M. Bardintzeff, J. Rasendrasoa, H. Bellon, C. Thouin, P. Gioan, and A. Piqué (1998), Rifting-related magmatic episodes of south-western Malagasy (Morondava basin), *C. R. Acad. Sci., Ser. II*, *326*, 685–691.

Ravenhurst, C. E., M. K. Roden-Tice, and D. S. Miller (2003), Thermal annealing of fission tracks in fluorapatite, chlorapatite, manganoapatite, and Durango apatite: Experimental results, *Can. J. Earth Sci.*, *40*, 995–1007, doi:10.1139/e03-032.

Razafimbelo, E. (1987), Le bassin de Morondava (Madagascar). Synthèse géologique et structural, PhD thesis, Univ. Louis Pasteur, Strasbourg, France.

Reeves, C., and M. de Wit (2000), Making ends meet in Gondwana: Retracing the transforms of the Indian Ocean and reconnecting continental shear zones, *Terra Nova*, *12*, 272–280, doi:10.1046/j.1365-3121.2000.00309.x.

Schandelmeier, H., F. Bremer, and H. Holl (2004), Kinematic evolution of the Morondava rift basin of SW Madagascar–from wrench tectonics to normal extension, *J. Afr. Earth Sci.*, *38*, 321–330, doi:10.1016/j.jafrearsci.2003.11.002.

Ségoufin, J., and P. Patriat (1980), Existence d'anomalies mésozoiques dans le basin de Somalie: Implications pour les relations Afrique-Antarctique-Madagascar, *C. R. Seances Acad. Sci., Ser. B*, *291*, 85–88.

Seward, D., D. Grujic, and G. Schreurs (1998), The exhumation history of the East Madagascar continental margin: Inferences from apatite fission-track analysis, *J. Afr. Earth Sci.*, *27*, 176–178.

Seward, D., D. Grujic, and G. Schreurs (1999), Exhumation history of southern Madagascar as revealed by zircon and apatite fission-track thermochronology, *Gondwana Res.*, *2*, 353–354, doi:10.1016/S1342-937X(05)70273-2.

Seward, D., D. Grujic, and G. Schreurs (2000a), Post Pan-African events in Madagascar: Inferences from apatite fission-track analysis, *Geol. Soc. Aust. Abstr.*, *58*, 289–290.

Seward, D., R. Spikings, G. Viola, A. Kounov, G. Ruiz, and N. Naeser (2000b), Etch times and operator variation for spontaneous track length measurements in apatite: An intra-laboratory check, *On Track*, *10*, 19–21.

Seward, D., D. Grujic, and G. Schreurs (2004), An insight into the breakup of Gondwana: Identifying events through low-temperature thermochronology from the basement rocks of Madagascar, *Tectonics*, *23*, TC3007, doi:10.1029/2003TC001556.

Sobel, E., and D. Seward (2010), Influence of etching conditions on apatite fission-track etch pit diameter, *Chem. Geol.*, *271*, 59–69, doi:10.1016/j.chemgeo.2009.12.012.

Stern, R. J. (1994), Arc assembly and continental collision in the Neoproterozoic East African Orogen: Implications for the consolidation of Gondwanaland, *Annu. Rev. Earth Planet. Sci.*, *22*, 319–351, doi:10.1146/annurev.ea.22.050194.001535.

Storey, B. C. (1995), The role of mantle plumes in continental breakup: Case-histories from Gondwanaland, *Nature*, *377*, 301–308, doi:10.1038/377301a0.

Storey, M., J. J. Mahoney, A. D. Saunders, R. A. Duncan, S. P. Kelley, and M. F. Coffin (1995), Timing of hot spot-related volcanism and the breakup of Madagascar and India, *Science*, *267*, 852–855, doi:10.1126/science.267.5199.852.

Storey, M., J. J. Mahoney, and A. D. Saunders (1997), Cretaceous basalts in Madagascar and the transition between plume and continental mantle sources, in *Large Igneous Provinces: Continental, Oceanic, and Planetary Flood Volcanism*, *Geophys. Monogr. Ser.*, vol. 100, edited by J. Mahoney and F. Coffin, pp. 95–122, AGU, Washington, D. C., doi:10.1029/GM100p0095.

Stüwe, K., and M. Hintermüller (2000), Topography and isotherms revisited: The influence of laterally migrating drainage divides, *Earth Planet. Sci. Lett.*, *184*, 287–303, doi:10.1016/S0012-821X(00)00315-0.

Stüwe, K., L. White, and R. Brown (1994), The influence of eroding topography on steady-state isotherms. Application to fission track analysis, *Earth Planet. Sci. Lett.*, *124*, 63–74, doi:10.1016/0012-821X(94)00068-9.

Torsvik, T. H., R. D. Tucker, L. D. Ashwal, E. A. Eide, N. A. Rakotosolofo, and M. J. de Wit (1998), Late Cretaceous magmatism in Madagascar: Palaeomagnetic evidence for a stationary Marion hotspot, *Earth Planet. Sci. Lett.*, *164*, 221–232, doi:10.1016/S0012-821X(98)00206-4.

Torsvik, T. H., R. D. Tucker, L. D. Ashwal, L. M. Carter, B. Jamtveit, K. T. Vidyadharan, and P. Venkataramana (2000), Late Cretaceous India-Madagascar fit and timing of break-up related magmatism, *Terra Nova*, *12*, 220–224, doi:10.1046/j.1365-3121.2000.00300.x.

Tucker, R. D., T. M. Kusky, R. Buchwaldt, and M. J. Handke (2007), Neoproterozoic nappes and superposed folding of the Itremo Group, west-central Madagascar, *Gondwana Res.*, *12*, 356–379, doi:10.1016/j.gr.2006.12.001.

Uhmann, A. (1996), Sedimentologische und fazielle Entwicklung in Jura und Kreide im Morondava Becken (Südwest-Madagaskar) - Untersuchungen zur Mikrofazies, Tongeologie und Schwermineralogie, PhD thesis, Tech. Univ. Berlin, Berlin.

UNESCO (1990), S-E Africa and Madagascar, in *International Geological Maps of Africa, scale 1:5.000.000, sheet 6*, Comm. for the Geol. Map of the World, Paris.

USGS (2004), 1 Arc Second scene SRTM_u03_n008e004, Unfilled Unfinished 2.0, Shuttle Radar Topography Mission, http://www.glcf.umd.edu/data/srtm/, Global Land Cover Facil., Univ. of Md., College Park, Md.

Wescott, W. A., and J. N. Diggens (1997), Depositional history and stratigraphical evolution of the Sakoa Group (Lower Karoo Supergroup) in the southern Morondava Basin, Madagascar, *J. Afr. Earth Sci.*, *24*, 585–601, doi:10.1016/S0899-5362(97)00082-1.

Wescott, W. A., and J. N. Diggens (1998), Depositional history and stratigraphical evolution of the Sakamena Group (Middle Karoo Supergroup) in the southern Morondava Basin, Madagascar, *J. Afr. Earth Sci.*, *27*, 461–479, doi:10.1016/S0899-5362(98)00073-6.

J. Giese, Louis Ingenieurgeologie GmbH, Weiherstr. 4, CH-6353 Weggis, Switzerland. (joerg.giese@uni-muenster.de)

G. Schreurs, Institute of Geological Sciences, University of Bern, Baltzerstr. 1, CH-3012 Bern, Switzerland.

D. Seward, School of Geography, Environment and Earth Sciences, Victoria University of Wellington, PO Box 600, Wellington 6012, New Zealand.